

Consistent Excesses in the Search for $\tilde{\chi}_2^0\tilde{\chi}_1^\pm$: Wino/bino vs. Higgsino Dark Matter

MANIMALA CHAKRABORTI^{1*}, SVEN HEINEMEYER^{2†} AND IPSITA SAHA^{3‡}

¹*School of Physics and Astronomy, University of Southampton, Southampton, SO17 1BJ, United Kingdom.*

²*Instituto de Física Teórica (UAM/CSIC), Universidad Autónoma de Madrid, Cantoblanco, 28049, Madrid, Spain*

³*Department of Physics, Indian Institute of Technology Madras, Chennai 600036, India*

Abstract

The quest for supersymmetric (SUSY) particles is among the main search channels currently pursued at the LHC. Particularly, electroweak (EW) particles with masses as low as a few hundred GeV are still viable. Recent searches for the “golden channel”, $pp \rightarrow \tilde{\chi}_2^0\tilde{\chi}_1^\pm \rightarrow \tilde{\chi}_1^0 Z^{(*)} \tilde{\chi}_1^0 W^{\pm(*)}$ show consistent excesses between ATLAS and CMS in the 2 lepton, 3-lepton and mono-jet searches, assuming $m_{\tilde{\chi}_2^0} \approx m_{\tilde{\chi}_1^\pm} \gtrsim 200$ GeV and $\Delta m := m_{\tilde{\chi}_2^0} - m_{\tilde{\chi}_1^0} \approx 20$ GeV. This mass configuration arises naturally in SUSY scenarios with wino/bino Dark Matter (DM) or higgsino DM. In these scenarios the lightest supersymmetric particle (LSP), assumed to be the lightest neutralino, $\tilde{\chi}_1^0$, as a DM candidate is in good agreement with the observed limits on the DM content of the universe, as well as with negative results from Direct Detection (DD) experiments. We analyze these two scenarios with respect to the observed excesses, taking into account all relevant experimental constraints. We show that in particular wino/bino DM with different signs of the $SU(2)$ and $U(1)$ soft SUSY-breaking parameters can describe well the experimental excesses, while being in agreement with all other constraints.

*email: M.Chakraborti@soton.ac.uk

†email: Sven.Heinemeyer@cern.ch

‡email: ipsita@iitm.ac.in

1 Introduction

Despite the remarkable success of the Standard Model (SM) in explaining the existing experimental data, the problem of Dark Matter (DM) remains unsolved till date. Therefore, one of the main objectives of today’s “direct detection” (DD) searches as well as collider-based experiments is to understand the nature and origin of DM. From the theoretical perspective, it is possible to construct a plethora of theories Beyond the Standard Model (BSM) containing a viable DM candidate. A leading candidate among them is the Minimal Supersymmetric (SUSY) Standard Model (MSSM) [1–4] (see Ref. [5] for a recent review), which remains as one of the most well-motivated scenarios for BSM physics. The MSSM extends the particle content of the SM by incorporating two scalar partners for all SM fermions as well as fermionic partners to all SM bosons. Furthermore, the MSSM requires the presence of two Higgs doublets, resulting in a rich structure in the Higgs sector with five physical Higgs bosons, instead of the single Higgs boson in the SM. These are the light and heavy \mathcal{CP} -even Higgs bosons (h and H), the \mathcal{CP} -odd Higgs boson (A), and a pair of charged Higgs bosons (H^\pm). The electroweak (EW) sector of the MSSM contains the SUSY partners of the SM leptons known as the scalar leptons (sleptons). Additionally, the neutral (charged) SUSY partners of the neutral (charged) Higgses and EW gauge bosons give rise to the four neutralinos, $\tilde{\chi}_{1,2,3,4}^0$ (two charginos, $\tilde{\chi}_{1,2}^\pm$), also called “EWinos”. In the MSSM with conserved R-parity, the lightest neutralino can become the lightest SUSY particle (LSP), yielding a good weakly interacting massive particle (WIMP) DM candidate [6, 7]. There exists a wide range of experimental searches already at the LHC looking for the production and decays of the EWinos and sleptons in various final states.

Some of the most effective constraints on the EW MSSM parameter space comes from the searches looking for the production of the heavier EWinos, $\tilde{\chi}_2^0$ and $\tilde{\chi}_1^\pm$, in final states containing two or three leptons accompanied by substantial missing transverse energy (\cancel{E}_T) [8, 9]. These searches become particularly challenging in the region of parameter space where the mass difference between the initial and final state EWinos become small, making the visible decay products, in this case leptons, to be rather soft. The ATLAS and CMS collaborations are actively searching for the EWinos in this “compressed spectra” region in soft dilepton and \cancel{E}_T final states. Interestingly, recent searches for the “golden channel”, $pp \rightarrow \tilde{\chi}_2^0 \tilde{\chi}_1^\pm \rightarrow \tilde{\chi}_1^0 Z^{(*)} \tilde{\chi}_1^0 W^{\pm(*)}$ show consistent excesses between ATLAS and CMS in the soft 2/3 lepton plus missing energy [10, 11], and combined 2/3 leptons plus missing energy [12, 13] searches assuming $m_{\tilde{\chi}_2^0} \approx m_{\tilde{\chi}_1^\pm}$ in the region $\Delta m := m_{\tilde{\chi}_2^0} - m_{\tilde{\chi}_1^0} \approx 20$ GeV. Similar excesses have also been reported in the mono-jet searches [14–16] around the same mass region. Therefore, it seems naturally interesting to identify the underlying parameter configuration of the EW MSSM and the associated properties of the EWinos that can give rise to such excesses at the LHC.

Previously, in Refs. [17–22] we performed a comprehensive analysis of the EW sector of the MSSM, taking into account all relevant theoretical and (then valid) experimental constraints. The experimental results comprised of the DM relic abundance [23], the DM direct detection (DD) experiments [24–26], the direct searches at the LHC [8, 9], as well as the discrepancy between the experimental result [27–29] for the anomalous magnetic moment of the muon,

$(g-2)_\mu$, and its SM prediction [30] (based on Refs. [31–50]). The latter is found either at the $\sim 5\sigma$ level, based on e^+e^- data, or at the $\sim 2\sigma$ level, based on lattice calculations [51].

In Refs. [17–22] six different scenarios were analyzed, classified by the mechanism that brings the LSP relic density into agreement with the measured values. The scenarios differ by the hierarchies among the mass scales determining the neutralino, chargino and slepton masses. The relevant mass scales that determine such hierarchies are the $U(1)$ and $SU(2)$ soft-SUSY breaking parameters M_1 and M_2 , the Higgs mixing parameter μ (where in Refs. [17–22] the three parameters were assumed to be positive) and the slepton soft SUSY-breaking parameters $m_{\tilde{l}_L}$ and $m_{\tilde{l}_R}$, where either all three generations of sleptons were assumed to be degenerate, or the third generation is independent of the first two.

The mass configuration favored by the experimental excesses in the compressed spectra search for EWkinos discussed above is naturally found in two of these scenarios:

- (i) wino/bino DM with $\tilde{\chi}_1^\pm$ -coannihilation ($|M_1| \lesssim |M_2| < |\mu|$),
- (ii) higgsino DM ($|\mu| < |M_1|, |M_2|$).

In this paper we analyze these two MSSM scenarios at the EW scale w.r.t. the consistent experimental excesses in the search $pp \rightarrow \tilde{\chi}_2^0 \tilde{\chi}_1^\pm \rightarrow \tilde{\chi}_1^0 Z^{(*)} \tilde{\chi}_1^0 W^{\pm(*)}$, taking into account all other relevant experimental constraints. We also demonstrate how future DD experiments can conclusively test these scenarios.

This paper is organized as follows. In Sect. 2 we briefly review the parameters of the EW sector of MSSM, fix our notations and define the two scenarios under investigation. The relevant constraints for this analysis, in particular the excesses in the searches for $\tilde{\chi}_2^0 \tilde{\chi}_1^\pm$ at the LHC, are summarized in Sect. 3. In Sect. 5 we present the details of our results as well as the prospects for future DD experiments. We conclude in Sect. 6.

2 The electroweak sector of the MSSM

In our MSSM notation we follow exactly Ref. [17]. Here we give a very short introduction of the relevant symbols and parameters, concentrating on the EW sector of the MSSM. We also compare with our previous studies [17–22] in regard to the choice of parameter region wherever applicable. The EW sector consists of charginos, neutralinos and scalar leptons. Following the experimental limits for strongly interacting particles from the LHC [8, 9], the colored sector particles are assumed sufficiently heavy such that it has no direct implications in our analysis. Furthermore, throughout this analysis we assume the absence of \mathcal{CP} -violation, i.e. that all parameters are real.

For the Higgs-boson sector it is assumed that the radiative corrections to the light \mathcal{CP} -even Higgs boson, which are dominated by the top/stop sector contributions, yield a value in agreement with the experimental data, $M_h \sim 125$ GeV. This results in stop masses that are naturally in the TeV range [54, 55], thus in agreement with the LHC bounds.

In the EW sector, the masses and mixings of the four neutralinos are given by (besides SM parameters) the $U(1)_Y$ and $SU(2)_L$ gaugino masses, M_1 and M_2 , the Higgs mixing parameter μ , as well as $\tan\beta := v_2/v_1$: the ratio of the two vacuum expectation values (vevs) of the two Higgs doublets. Diagonalizing the mass matrix yields the four eigenvalues for the neutralino masses $m_{\tilde{\chi}_1^0} < m_{\tilde{\chi}_2^0} < m_{\tilde{\chi}_3^0} < m_{\tilde{\chi}_4^0}$. Similarly, the masses and mixings of the charginos are given by (besides SM parameters) by M_2 , μ and $\tan\beta$. Diagonalizing the mass matrix yields the two eigenvalues for the chargino-masses, $m_{\tilde{\chi}_1^\pm} < m_{\tilde{\chi}_2^\pm}$.

For the sleptons, as in Refs. [17–21], but contrary to Ref. [22], we have chosen common soft SUSY-breaking parameters for all three generations. The mass matrices of the charged sleptons are determined by the diagonal soft SUSY-breaking parameters $m_{\tilde{l}_L}^2$ and $m_{\tilde{l}_R}^2$ and the trilinear Higgs-slepton coupling A_l ($l = e, \mu, \tau$), where the latter are set to zero. Consequently, the mass eigenvalues can be approximated as $m_{\tilde{l}_1} \simeq m_{\tilde{l}_L}, m_{\tilde{l}_2} \simeq m_{\tilde{l}_R}$ (assuming small D -terms). We do not mass order the sleptons, i.e. we follow the convention that \tilde{l}_1 (\tilde{l}_2) has the large “left-handed” (“right-handed”) component. The sneutrino and slepton masses are connected by the usual $SU(2)$ relation.

Overall, the EW sector at the tree level can be described with the help of six parameters: $M_1, M_2, \mu, \tan\beta, m_{\tilde{l}_L}, m_{\tilde{l}_R}$. We assume $\mu, M_2 > 0$ throughout our analysis, but allow for positive and negative M_1 . This is in contrast to Refs. [17–22], where all parameters were assumed to be positive. While the latter is sufficient to cover the relevant contributions to $(g-2)_\mu$, allowing for $\mu \times M_1 < 0$ can yield lower DM DD rates (see, e.g., the discussion in Ref. [52, 53]), and can have important consequences for the chargino/neutralino production cross sections at the LHC, see the discussion below.

Contrary to our previous analyses [17–22], the heavy \mathcal{CP} -even Higgs boson can play a relevant role in the (cancellation of the) contributions to the DD cross sections, where both the h and H exchange can contribute. This becomes relevant especially for higgsino DM. Here, particularly interesting is the case of $\mu \times M_1 < 0$ (we restrict ourselves to $\mu > 0$)¹, where the two contributions of h and H can cancel. Consequently, we leave M_A as an additional free parameter in the higgsino scenario. This requires, in principle, to check the Higgs-boson sector against experimental constraints from the BSM Higgs-boson searches, as well as the LHC Higgs-boson rate measurements, as will be discussed below.

3 Experimental constraints

Here we briefly list the experimental constraints that we apply to our data sets.

- Anomalous magnetic moment of the muon:

¹This choice yields a positive SUSY contribution to $(g-2)_\mu$ [56–59], corresponding to our original motivation, see also the discussion in the next section.

The original motivation of our series of analyses [17–22] was the discrepancy between the SM prediction[30] (based on Refs. [31–50]) and the experimental measurement of a_μ [27–29]. Compared with the new experimental result, the deviation results to

$$\Delta a_\mu = (24.9 \pm 4.8) \times 10^{-10}, \quad (1)$$

corresponding to a $\sim 5\sigma$ discrepancy. However, this result does not incorporate the lattice calculation [51] for the leading order hadronic vacuum polarization (LO HVP) contribution. Inclusion of this theory prediction would yield a slightly higher value for a_μ^{SM} leading to a smaller deviation from the experimental result of $\lesssim 2\sigma$. This result is partially supported by some other lattice calculations [60, 61].

In the MSSM the dominant SUSY contribution to $(g-2)_\mu$ at one-loop originates from the gaugino-slepton loops [56–59]. For our analysis we evaluate the MSSM contribution to $(g-2)_\mu$ based on a full one-loop plus partial two-loop calculation [62–64] (see also [65, 66]), as implemented into the code `GM2Calc` [67].

In this work, we deliberately choose the sleptons to be heavier than the neutralinos and the charginos to be consistent with the assumptions made in the experimental searches for $pp \rightarrow \tilde{\chi}_2^0 \tilde{\chi}_1^\pm$. We note, however, that with higher values of slepton masses, a_μ can easily be adjusted to yield the $\lesssim 2\sigma$ discrepancy as suggested by Ref. [51] without changing the results of our analysis. On the other hand, only the wino/bino scenarios can comply with the constraint of Eq. (1) within $\pm 2\sigma$ uncertainty in the preferred mass configuration. More details are given in Sect. 4.

- Vacuum stability constraints:

For the higgsino scenario, by choosing heavier sleptons and all slepton trilinear couplings set to zero, the scalar potential is not influenced in a relevant way by the slepton sector. Consequently, vacuum stability constraints are naturally fulfilled. For the wino/bino scenarios, our parameter points are checked against vacuum stability constraints allowing for the possibility of a metastable universe [68–72].

- DM relic density constraints:

the latest result from the Planck experiment [23] provides the experimental data. The relic density is given by,

$$\Omega_{\text{CDM}} h^2 = 0.120 \pm 0.001, \quad (2)$$

which we use as a measurement of the full density given by the LSP, or as an upper bound (calculated using the central value with 2σ upper limit),

$$\Omega_{\text{CDM}} h^2 \leq 0.122. \quad (3)$$

The calculation of the relic density in the MSSM is performed with `MicrOMEGAs` [73–76].

- DM direct detection constraints:

We use the latest limit on the spin-independent (SI) DM scattering cross-section σ_p^{SI} from the LZ [77] experiment. We have checked that our parameter points also satisfy

the spin-dependent direct detection limits [77]. The theoretical predictions are calculated using `MicrOMEGAs` [73–76]. Apart from this limit we will discuss the impact of projected Xenon-nT/LZ [104, 105] limits and the neutrino floor reach.

For parameter points with $\Omega_{\tilde{\chi}} h^2 \leq 0.118$, i.e. with underabundant relic density, the DM scattering cross-section is rescaled with a factor of $(\Omega_{\tilde{\chi}} h^2 / 0.118)$. In this way it is taken into account that the $\tilde{\chi}_1^0$ provides only a fraction of the total DM relic density of the universe.

For the higgsino case, the DD constraint is particularly relevant. As shown in Ref. [18], it cuts away $\Delta m \gtrsim 10$ GeV, i.e. the region of interest, if not a cancellation of the h and H exchange contributions in SI DD cross section occurs. As shown in Ref. [78], such a cancellation can happen for $\mu \times M_1 < 0$. In the limit of large M_2 an exact cancellation occurs for

$$\mu = \frac{-2M_1 \tan \beta}{4 + M_h^2 / M_H^2 \tan^2 \beta} . \quad (4)$$

However, also small deviations from Eq. (4) can yield a sufficiently small DD cross section, where $\mu < |M_1|$ provides an upper bound from the requirement of higgsino-dominated DM. On the other hand, in the wino/bino scenario considered here, the non-standard Higgs bosons do not play a significant role and therefore their masses are assumed to be beyond the reach of the LHC.

However, the viability of the higgsino scenario relies on a reduced DD cross section realized by a cancellation of the h and H exchange contributions to the SI DD cross section (see the discussion above). This in turn requires a not-too-large heavy Higgs-boson mass scale, M_A . This will be relevant in view of the BSM Higgs-boson searches and the LHC Higgs-boson rate measurements discussed below.

- Indirect DM detection:

Another potential set of constraints is given by the indirect detection of DM. We do not, however, impose these constraints on our parameter space because of the well-known large uncertainties associated with astrophysical factors (e.g. DM density profile, theoretical corrections etc., see Refs. [79–82]). The most precise indirect detection limits come from DM-rich dwarf spheroidal galaxies, where the uncertainties on the cross section limits are found in the range of $\sim 2 - 3$ [83, 84]. The most strict constraint from the latest analysis [83] assuming only one single dominant DM annihilation mode, sets a limit as $m_{\tilde{\chi}_1^0} \gtrsim 100$ GeV, for a generic thermal relic saturating Eq. (2). This limit is much weaker than all other experimental constraints considered in this study.

- Constraints from LHC Higgs-boson rate measurements:

Any model beyond the SM has to accommodate a Higgs boson with mass and signal strengths as they were measured at the LHC. The mass of the lightest \mathcal{CP} -even Higgs-boson, h , is assumed to be $M_h \sim 125$ GeV, i.e. in agreement with the LHC measurements [85]. The properties of the lightest \mathcal{CP} -even Higgs are driven by M_A and $\tan \beta$ at the tree-level. While we leave these two parameters free, in principle, it has been shown (see, e.g., Ref. [86]) that for $M_A \gtrsim 500$ GeV the production and decay rates of h closely resemble their SM values and are thus in sufficient agreement with

the LHC measurements. Additionally, as previously mentioned, the mass parameters of the colored sector have been set to large values, moving these particles outside the reach of the LHC sensitivity. However, this sector, in particular, the scalar tops and bottoms, can influence the properties of the h (see Ref. [55] for a recent review) via loop corrections. In order to keep the parameter space at a level that can be analyzed without too high computational costs, we remain agnostic about the parameters of the colored sector. Furthermore, we will demand a lower limit of $M_A \gtrsim 500$ GeV to yield agreement with the LHC rate measurements, where M_A may have significant implications (see the DD constraints above), or fix it to a definite value where it has no direct impact.

Another possible source for large effects beyond the SM are additional loop contributions in the loop-induced process $h \rightarrow \gamma\gamma$. Here in particular a light chargino can yield large corrections. However, the correction will only be significant to future sensitivities of ATLAS and CMS. The current uncertainties in the $\text{BR}(h \rightarrow \gamma\gamma)$ measurements are too large to provide any relevant constraints [87].

- Constraints from direct Higgs-boson searches at the LHC:
As argued above, the viability of the higgsino scenario relies on a reduced DD cross section realized by a cancellation of the h and H exchange contributions to the SI DD cross section, requiring a not-too-large heavy Higgs-boson mass scale, M_A . This makes these Higgs bosons subject to the ongoing BSM searches at the LHC. However, as argued above, the parameter space with $M_A \lesssim 500$ GeV is inconsistent the LHC Higgs-boson rate measurements. On the other hand, as will be demonstrated below, the higher values appear to be inconsistent with a description of the experimental excesses. Consequently, we do not have to test the higgsino parameter space against the BSM Higgs-boson searches at the LHC.
- Constraints from flavor physics:
Constraints from flavor physics can be particularly sensitive to charged Higgs boson contributions [88, 89]. Here the decays $B \rightarrow X_s \gamma$ and $B_s \rightarrow \mu^+ \mu^-$ are most relevant. With our choice of M_A (see above) and the charged Higgs-boson mass being close to M_A ($M_{H^\pm} \sim M_A$), these mass scales are too large to contribute relevantly to the flavor constraints [89, 90].
- Searches for EWinos and sleptons at the LHC:
In this analysis we are interested in the $\tilde{\chi}_2^0\text{-}\tilde{\chi}_1^\pm$ pair production searches with decays via $Z^{(*)}$ and $W^{(*)}$ into final states involving 2-3 leptons and large \cancel{E}_T . The latest ATLAS analysis [12] corresponding to the full Run 2 dataset with 139 fb^{-1} of luminosity targets 3 leptons and \cancel{E}_T final state. It also provides a statistical combination with the previous ATLAS search targeting the “compressed spectra” region in the soft 2 leptons and \cancel{E}_T final state [10]. The simplified SUSY models considered in Ref. [12] are the wino/bino and higgsino scenarios. In the wino/bino scenario, $\tilde{\chi}_1^0$ is considered to be purely bino whereas $\tilde{\chi}_1^\pm$ and $\tilde{\chi}_2^0$ are taken to be purely wino and mass-degenerate. Two separate exclusion limits are provided for wino/bino(+) and wino/bino(-) scenarios, where the (+/-) indicates the relative sign of the parameters M_1 and M_2 , giving the dominant contribution to the $\tilde{\chi}_1^0$ and $\tilde{\chi}_2^0/\tilde{\chi}_1^\pm$ mass eigenstates. The higgsino simplified

model assumes $\tilde{\chi}_2^0$, $\tilde{\chi}_1^0$ and $\tilde{\chi}_1^\pm$ to be higgsino-like states with $m_{\tilde{\chi}_1^\pm}$ lying midway between $m_{\tilde{\chi}_1^0}$ and $m_{\tilde{\chi}_2^0}$. The reported deficits in the observed versus the expected exclusion appear in the region $\Delta m := m_{\tilde{\chi}_2^0} - m_{\tilde{\chi}_1^0} \approx 10\text{--}30$ GeV, corresponding to $\tilde{\chi}_1^\pm$ ($\tilde{\chi}_2^0$) decaying via an off-shell $W(Z)$ plus a $\tilde{\chi}_1^0$, for which 100% branching ratio is assumed in both the simplified models.

The latest analyses from CMS collaboration [13] targeting the wino/bino simplified model provides a statistically combined exclusion limit involving “2/3l soft” and $\geq 3l$ signal regions. The exclusion limit for the higgsino simplified model in the “2/3l soft” channel is presented in Ref. [11]. The deficits in the observed exclusion limits compared to the expected limits is obtained in the region $\Delta m \approx 20 - 50$ GeV for wino/bino and $\Delta m \approx 8 - 20$ GeV for higgsino simplified models. In our analysis we impose these limits directly on our wino/bino and higgsino model parameter space as a conservative approximation. It should be noted here that, in principle, the production cross section and the branching ratios may not comply strictly with the simplified model assumptions made by the experimental groups. Further explanation on this will be discussed in Sect. 5.4.

In Fig. 1 we show the ATLAS and CMS results for the wino/bino(+) scenario (i.e. with $M_1 \times M_2 > 0$) in the upper left plot, for the wino/bino(-) scenario (i.e. with $M_1 \times M_2 < 0$) in the upper right plot, and for the higgsino(-) scenario (i.e. with $M_1 \times \mu < 0$) in the lower plot. The limits are displayed in the $m_{\tilde{\chi}_2^0} - \Delta m := m_{\tilde{\chi}_2^0} - m_{\tilde{\chi}_1^0}$ plane. The ATLAS (CMS) expected exclusions are shown in gray (teal), where the bands indicate the experimental 1σ uncertainties. The observed limits for ATLAS (CMS) are shown in black (brown), where the bands indicate the 1σ theory uncertainties. As discussed above, the observed limits are in all cases weaker than the expected ones. In the wino/bino(+) scenario it can be observed that both results exhibit an excess of events, corresponding to lower excluded $m_{\tilde{\chi}_2^0}$ values as compared to their expected limits. For ATLAS the excess is most pronounced for $\Delta m \sim 15$ GeV, while for CMS it is found for ~ 30 GeV. However, the mass resolution is at the ~ 5 GeV, and thus the two excesses appear still compatible with each other. In the wino/bino(-) scenario one can see that both results exhibit an excess of events. For ATLAS the excess is most pronounced for $\Delta m \sim 25$ GeV, while for CMS it is found for slightly higher values of ~ 30 GeV. Both excesses are well compatible with each other (or even slightly better than in the wino/bino(+) case). In the higgsino(-) scenario the ATLAS excess is most pronounced at $\Delta m \sim 30$ GeV, while CMS shows an excess of events in the range $\Delta m = 20 - 30$ GeV.

In our wino/bino scenario, the possibility of accommodating the $(g - 2)_\mu$ anomaly at the $\sim 5\sigma$ level requires the slepton masses to be sufficiently light. This makes these scenarios subject to the bounds from slepton-pair production searches leading to two same flavour opposite sign leptons and \cancel{E}_T in the final state [91]. We take this search into account with the help of the public tool `CheckMATEv2` [92–94] (Ref. [17] details many analyses newly implemented in `CheckMATEv2` by our group).

On the other hand, as discussed above, the contribution to $(g - 2)_\mu$ can be reduced to the $\sim 2\sigma$ level (or even below) by making the sleptons heavier. Since the sleptons do not play any role in the EWino searches discussed above, these additional test for

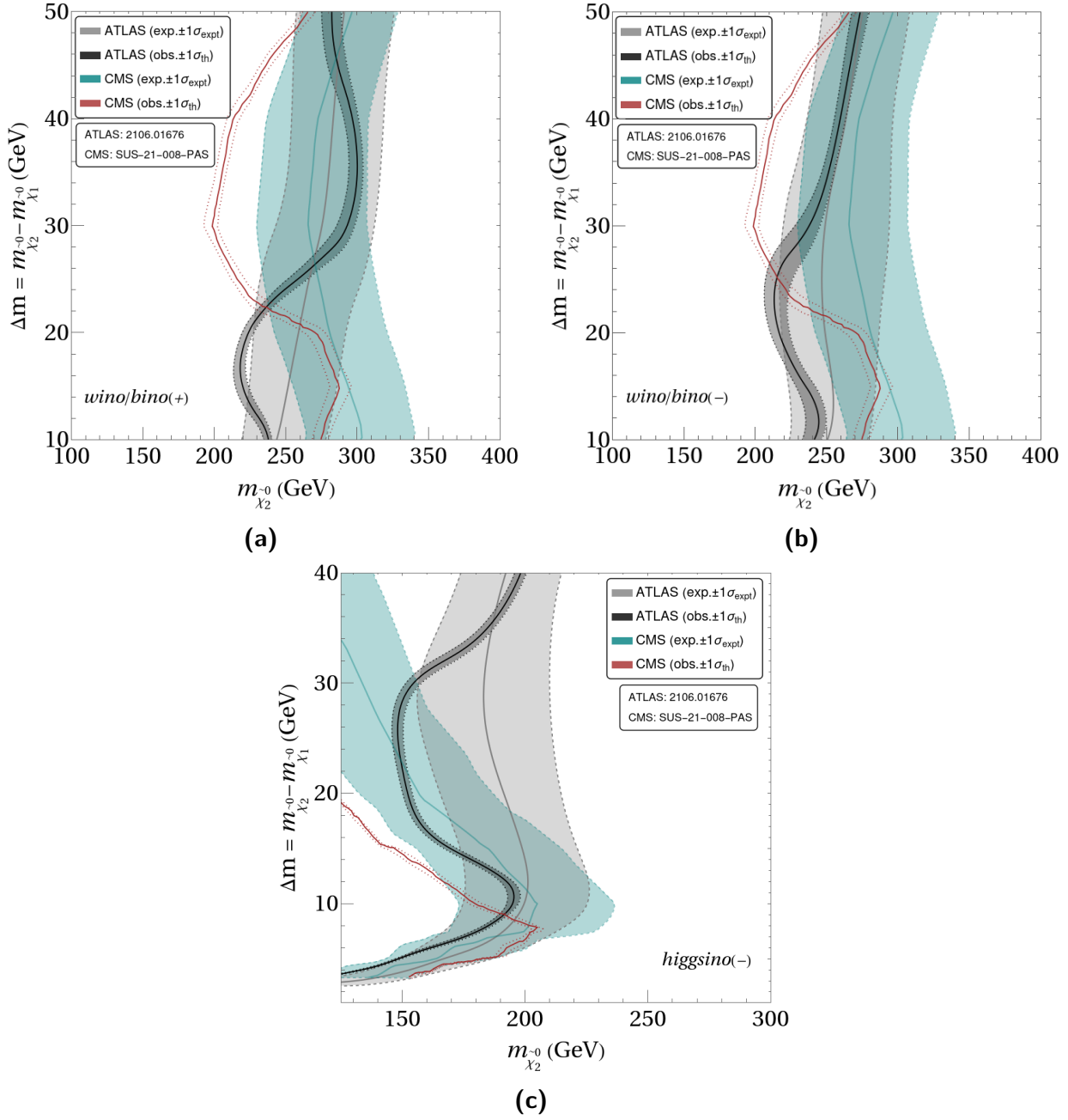


Figure 1: The experimental observed and expected limits with $\pm 1\sigma$ uncertainty (see text) for the three scenarios considered in this analysis.

light sleptons do not have any impact on our results if only a $\sim 2\sigma$ discrepancy for $(g-2)_\mu$ is considered.

4 Parameter scan and flow of the analysis

We scan the EW MSSM parameter space, fully covering the regions of low mass charginos and neutralinos. The sleptons can be light, but as discussed above, depending on their mass, either $\sim 5\sigma$ discrepancy, or the $\sim 2\sigma$ discrepancy of $(g-2)_\mu$ can be realized. We cover the three scenarios discussed above, leaving out higgsino DM with $\mu \times M_1 > 0$, since no cancellations in the DD cross sections can occur, which are relevant to allow for a sufficiently large Δm . The three scenarios are defined as follows.

wino/bino(+): wino/bino DM with $\mu \times M_1 > 0$

$$\begin{aligned} 100 \text{ GeV} \leq M_1 \leq 400 \text{ GeV} , \quad |M_1| \leq M_2 \leq 1.1 |M_1| , \\ 1.1 |M_1| \leq \mu \leq 10 |M_1| , \quad 2 \leq \tan \beta \leq 60 , \\ 100 \text{ GeV} \leq m_{\tilde{l}_L} = m_{\tilde{l}_R} \leq 1.5 \text{ TeV} , \quad M_A = 1.5 \text{ TeV} . \end{aligned} \quad (5)$$

wino/bino(-): wino/bino DM with $\mu \times M_1 < 0$

$$\begin{aligned} 100 \text{ GeV} \leq -M_1 \leq 400 \text{ GeV} , \quad |M_1| \leq M_2 \leq 1.4 |M_1| , \\ 1.2 |M_1| \leq \mu \leq 2 \text{ TeV} , \quad 2 \leq \tan \beta \leq 60 , \\ 100 \text{ GeV} \leq m_{\tilde{l}_L} = m_{\tilde{l}_R} \leq 1.5 \text{ TeV} , \quad M_A = 3 \text{ TeV} . \end{aligned} \quad (6)$$

higgsino(-): higgsino DM with $\mu \times M_1 < 0$

$$\begin{aligned} 190 \text{ GeV} \leq -M_1 \leq 1500 \text{ GeV} , \quad M_2 = 3 \text{ TeV} , \\ \frac{-2M_1 \tan \beta}{4 + M_h^2/M_H^2 \tan^2 \beta} \leq \mu \leq |M_1| , \\ 1 \leq \tan \beta \leq 50 , \\ m_{\tilde{l}_L} = m_{\tilde{l}_R} = 1.5 \text{ TeV} , \\ 190 \text{ GeV} \leq M_A \leq 1.5 \text{ TeV} . \end{aligned} \quad (7)$$

In the last scenario we scan over smaller M_A values to analyze the dependence on this parameter, see, however, our corresponding discussion on the LHC Higgs-boson rate measurements. Additionally, we fix the slepton masses at 1.5 TeV in this scenario. As we will see in Sect. 5.3, the requirement of simultaneously satisfying the DD constraints and the LHC searches for $pp \rightarrow H/A \rightarrow \tau^+\tau^-$ pushes us towards the region $\tan \beta \lesssim 2.5$. With such low values of $\tan \beta$, it becomes impossible to accommodate the $(g-2)_\mu$ discrepancy as given in Eq. (1). Since the sleptons are relevant only for the explanation of the $(g-2)_\mu$ anomaly without playing any role in the explanation of the excesses, we fix the slepton masses to sufficiently large values in the higgsino scenario without affecting the main result of our analysis. As discussed above, the mass parameters of the colored sector have been set to high values, moving these particles outside the reach of the LHC.

The three data samples were generated by scanning randomly over the input parameter ranges given above, assuming a flat prior for all parameters, generating $\mathcal{O}(10^7)$ points. The

code `SuSpect-v2.43` [95, 96] has been used as spectrum and SLHA file generator. In this step we also ensure that all points satisfy the slepton and $\tilde{\chi}_1^\pm$ mass limits from LEP [97]. The SLHA output files as generated by `SuSpect` are subsequently passed as input files to `MicrOMEGAs-v5.2.13` and `GM2Calc-v2.1.0` for the calculation of the DM observables and $(g-2)_\mu$, respectively. The parameter points that satisfy the $(g-2)_\mu$ constraint of Eq. (1) (note, however, the option of heavier sleptons), the DM relic density constraint of Eq. (2) or (3) and the DD constraints (possibly with a rescaled cross section) are tested. In this step also the vacuum stability constraints are checked. As a final step the LHC constraints are applied, either as implemented in `CheckMATEv2`, or directly for the bounds of interest from the $pp \rightarrow \tilde{\chi}_2^0 \tilde{\chi}_1^\pm$ search with low Δm . The relevant branching ratios of the SUSY particles (needed for the `CheckMATEv2` test) are calculated using `SDECAY-v1.5a` [98].

5 Results

We follow the analysis flow as described above and indicate the points surviving certain constraints with different colors:

- grey (round): all scan points.
- green (round): all points that are in agreement with $(g-2)_\mu$, taking into account the limit as given in Eq. (1), but that are excluded by the DM relic density. These points are only shown in the wino/bino(+) and wino/bino(-) scenario.
- blue (triangle): points that additionally give the correct DM relic density, see Sect. 3, but are excluded by the DD constraints.
- cyan (diamond): points that additionally pass the DD constraints, see Sect. 3, but are excluded by the LHC constraints (either by `CheckMATEv2`, or by the direct application of the searches of interest).
- red (star), only used for wino/bino(+) and wino/bino(-): points that additionally pass the LHC constraints, and that, in particular, give a match to the LHC searches $pp \rightarrow \tilde{\chi}_2^0 \tilde{\chi}_1^\pm$ with small Δm .
- magenta (star), only used for higgsino(-): same as cyan, but in addition the points pass the search $pp \rightarrow H/A \rightarrow \tau^+ \tau^-$ (the $(g-2)_\mu$ constraint is not applied).
- brown (star): only used for higgsino(-): same as magenta, but in addition $M_A > 500$ GeV is required (the $(g-2)_\mu$ constraint is not applied).

5.1 Preferred parameter ranges: wino/bino(+)

We start our phenomenological analysis with the case of wino/bino DM with $M_1 \times \mu > 0$. In this scenario M_2 is close to M_1 , defining the NLSP and ensuring the $\tilde{\chi}_1^\pm$ -coannihilation mechanism.

In Fig. 2 we show the result of our parameter scan in the wino/bino(+) case in the $m_{\tilde{\chi}_2^0} - \Delta m$ plane ($\Delta m = m_{\tilde{\chi}_2^0} - m_{\tilde{\chi}_1^0}$) (upper right), the $m_{\tilde{\chi}_1^0} - m_{\tilde{\chi}_2^0}$ plane (upper left), the $m_{\tilde{\chi}_1^0} - m_{\tilde{\mu}_1}$ plane (lower left), and the $m_{\tilde{\chi}_1^0} - \tan \beta$ plane (lower right). The points shown here are based on the analysis of the $\tilde{\chi}_1^\pm$ -coannihilation scenario in Ref. [19]. The main result can be seen in the upper left plot of Fig. 2. In the $m_{\tilde{\chi}_2^0} - \Delta m$ plane we compare the points found in our scan with the two main experimental limits for the search $pp \rightarrow \tilde{\chi}_2^0 \tilde{\chi}_1^\pm \rightarrow \tilde{\chi}_1^0 Z^* \tilde{\chi}_1^0 W^{\pm*}$ obtained at ATLAS and CMS in the wino/bino(+) scenario, see our discussion in Sect. 3. We only show the observed experimental limits, where for each Δm the stronger limit is indicated, including the 1σ theory uncertainties (with the same color coding as in Fig. 1). Following the color coding as detailed in the beginning of this section, we show in red the points that are in agreement with all constraints, as well as with both the LHC search limits from ATLAS and CMS. These are located at $m_{\tilde{\chi}_2^0} \gtrsim 250$ GeV (with the highest value reaching up to ~ 450 GeV in our scan), and have a Δm of about 18 GeV \dots 25 GeV. While the ATLAS excess is well described, the CMS excess would prefer slightly higher values of Δm (minding the experimental uncertainties in Δm).

The results of our scan are presented in the $m_{\tilde{\chi}_1^0} - m_{\tilde{\chi}_1^\pm}$ plane, shown in the upper right plot of Fig. 2. The wino/bino(+) scenario features $\tilde{\chi}_1^\pm$ -coannihilation and thus naturally has $m_{\tilde{\chi}_2^0} \sim m_{\tilde{\chi}_1^\pm} \sim m_{\tilde{\chi}_1^0} + \Delta m$ with a small Δm , see also Eq. (5). With the Δm values preferred from the ATLAS and CMS searches, we find the corresponding linear relation in the $m_{\tilde{\chi}_1^0} - m_{\tilde{\chi}_1^\pm}$ plane. The values range from $(m_{\tilde{\chi}_1^0}, m_{\tilde{\chi}_1^\pm}) \sim (230 \text{ GeV}, 250 \text{ GeV})$ up to $\sim (430 \text{ GeV}, 450 \text{ GeV})$.

The lower left plot of Fig. 2 presents the results in the $m_{\tilde{\chi}_1^0} - m_{\tilde{\mu}_1}$ plane, where in our scan, for sake of simplicity, we have set $m_{\tilde{\mu}_1} \approx m_{\tilde{\mu}_2} \approx m_{\tilde{e}_1} \approx m_{\tilde{e}_2}$. We find the whole allowed mass range $\sim 350 \text{ GeV} \lesssim m_{\tilde{\mu}_1} \lesssim 850 \text{ GeV}$. This is driven by the requirement to describe the $\sim 5\sigma$ deviation in $(g-2)_\mu$, see Eq. (1). However, as discussed above, we also require the sleptons to be heavier than the lighter neutralinos and charginos, such that they do not play a role in the experimental search for $pp \rightarrow \tilde{\chi}_2^0 \tilde{\chi}_1^\pm$. By choosing higher values of the slepton masses, the SUSY contribution to a_μ can easily be adjusted to yield the $\lesssim 2\sigma$ discrepancy as suggested by Ref. [51] without changing the results of our analysis.

In the lower right plot of Fig. 2 the results are shown in the $m_{\tilde{\chi}_1^0} - \tan \beta$ plane. Allowed points are found for $\tan \beta \gtrsim 20$ up to the scan limit of 60. In general, larger $\tan \beta$ values allow larger $m_{\tilde{\chi}_1^0}$, based on $(g-2)_\mu$. Lower $\tan \beta$ would be allowed for a 2σ discrepancy in $(g-2)_\mu$. The black line corresponds to $m_{\tilde{\chi}_1^0} = M_A/2$, i.e. roughly to the requirement for A -pole annihilation, where points above the black lines are experimentally excluded [86]. No valid points below the black line are found, excluding the possibility that A -pole annihilation place a role in the $\tilde{\chi}_1^\pm$ -coannihilation scenario.

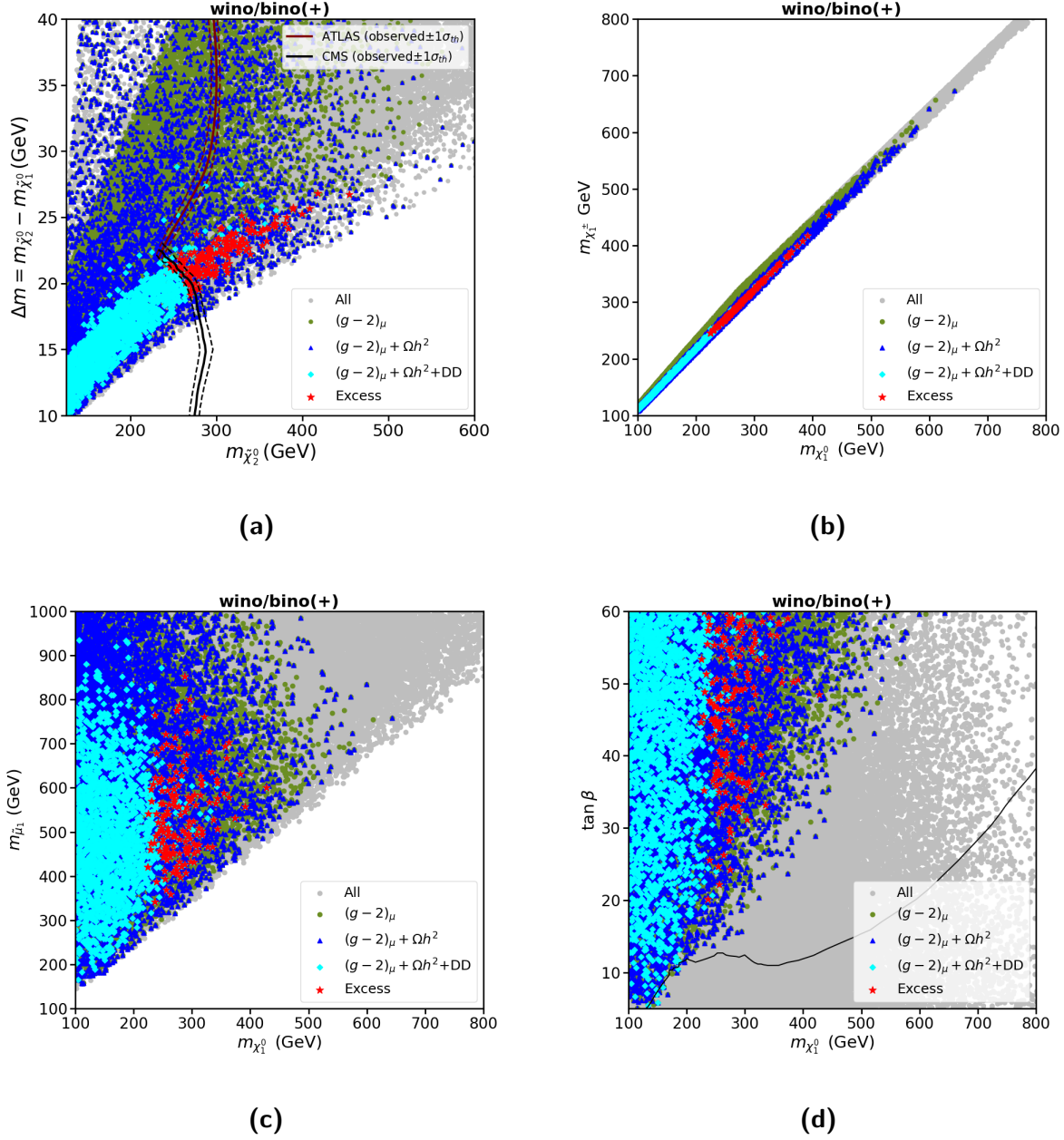


Figure 2: The results of our parameter scan in the wino/bino(+) case in the $m_{\tilde{\chi}_2^0}$ - Δm plane ($\Delta m = m_{\tilde{\chi}_2^0} - m_{\tilde{\chi}_1^0}$) (upper right), the $m_{\tilde{\chi}_1^0}$ - $m_{\tilde{\chi}_2^0}$ plane (upper right), the $m_{\tilde{\chi}_1^0}$ - $m_{\tilde{\mu}_1}$ plane (lower left), and the $m_{\tilde{\chi}_1^0}$ - $\tan \beta$ plane (lower right).

The cross section for $pp \rightarrow \tilde{\chi}_2^0 \tilde{\chi}_1^\pm$ at the LHC at $\sqrt{s} = 13$ TeV is shown in the $m_{\tilde{\chi}_2^0}$ - Δm plane in Fig. 3. We calculated the NLO+NLL threshold resummed cross sections at the LHC using the public package `Resummino` [99–103]. The results are shown only for points passing all constraints (the red points in Fig. 2). The size of the cross section for each point is indicated by the color scale. One can see that the cross section mainly depends on

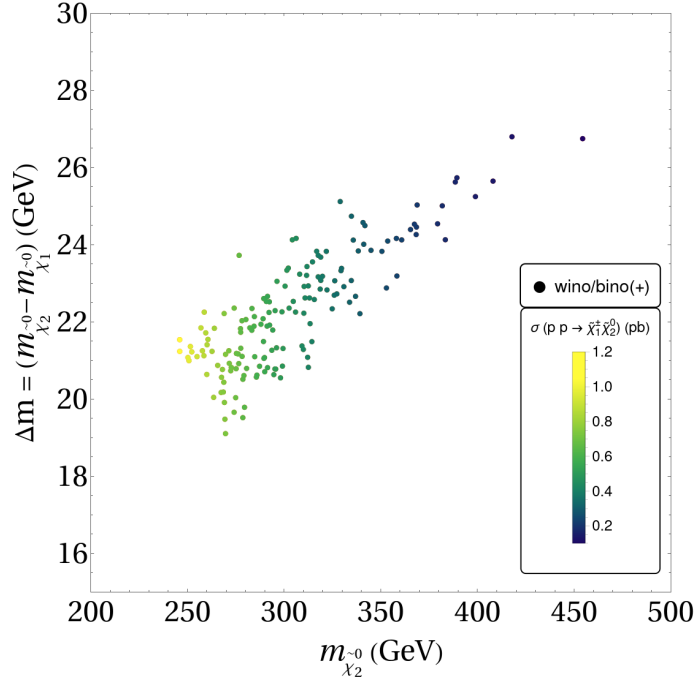


Figure 3: The results of our parameter scan in the wino/bino(+) scenario in the $m_{\tilde{\chi}_2^0} - \Delta m$ plane. Shown are only points allowed by all constraints. The color coding indicates the cross sections at the LHC at $\sqrt{s} = 13$ TeV.

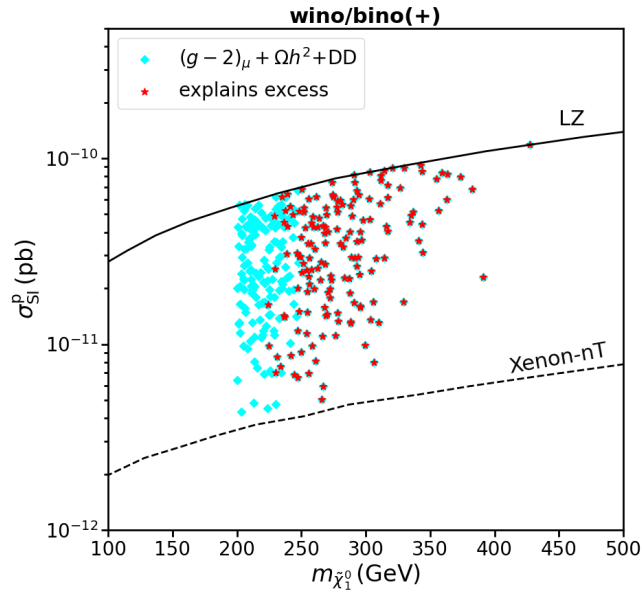


Figure 4: The results of our parameter scan in the wino/bino(+) scenario in the $m_{\tilde{\chi}_1^0} - \sigma_p^{\text{SI}}$ plane. Shown are only points allowed by DD limits (cyan and red).

$m_{\tilde{\chi}_2^0} \approx m_{\tilde{\chi}_1^\pm}$, but is nearly independent on Δm . The smallest EWino masses yield production cross sections of ~ 1 pb, going down to ~ 0.2 pb for the highest mass values. This roughly agrees with the cross sections needed to produce the observed excess in events (taking into account all uncertainties). On the other hand, this defines a target for the Run 3 of the LHC and beyond. While we are not aware of any projections for the discovery potential at the HL-LHC, following the results shown in Fig. 22 of Ref. [18], it appears possible that the points describing the excesses with largest $m_{\tilde{\chi}_2^0}$ can possibly escape the searches at the HL-LHC. However, these points with the highest $m_{\tilde{\chi}_2^0}$ values have correspondingly low cross sections, possibly too low to fully explain the observed excesses.

The future prospects for DD experiments are presented in Fig. 4. In the $m_{\tilde{\chi}_1^0}-\sigma_p^{\text{SI}}$ plane we only show the points in agreement with the constraints up to the DM DD constraint in cyan, and the points that additionally describe the LHC limits along with the ATLAS and CMS excesses in red (i.e. for the shown points we use the same color coding as in Fig. 2). The upper limit in the plot on the DD cross section is given by LZ [77]. Also indicated is the projected reach of Xenon-nT [104], which effectively agrees with the projected reach of LZ [105]. It can be seen that all allowed (red) points are above the projected Xenon-nT/LZ limit. Consequently, if the wino/bino(+) scenario is the correct description of the ATLAS and CMS excesses, we can expect these experiments will show a positive DM signal in the coming years.

We do not discuss in detail the prospects at future e^+e^- collider experiments, such as ILC or CLIC. Following the evaluations in Refs. [106, 107] and the cross section calculations shown in Refs. [17–20, 22] all charginos and neutralinos within the kinematical reach can be probed and discovered at high-energy (linear) e^+e^- colliders. In the wino/bino(+) scenario a center-of-mass energy of $\sqrt{s} \lesssim 1000$ GeV is sufficient to conclusively test this scenario.

5.2 Preferred parameter ranges: wino/bino(-)

We continue our phenomenological analysis with the case of wino/bino DM with $M_1 \times \mu < 0$. In this scenario the M_2 is close to $|M_1|$, defining the NLSP and ensuring the $\tilde{\chi}_1^\pm$ -coannihilation mechanism.

In Fig. 5 we show the result of our parameter scan in the wino/bino(-) case in the $m_{\tilde{\chi}_2^0}-\Delta m$ plane ($\Delta m = m_{\tilde{\chi}_2^0} - m_{\tilde{\chi}_1^0}$) (upper right), the $m_{\tilde{\chi}_1^0}-m_{\tilde{\chi}_2^0}$ plane (upper left), the $m_{\tilde{\chi}_1^0}-m_{\tilde{\mu}_1}$ plane (lower left), and the $m_{\tilde{\chi}_1^0}-\tan\beta$ plane (lower right). The points shown here are based on a new parameter scan, since in our previous analyses the scenarios with $M_1 \times \mu < 0$ was not covered. The main result can be seen in the upper left plot of Fig. 5. In the $m_{\tilde{\chi}_2^0}-\Delta m$ plane we compare the points found in our scan with the two main experimental limits for the search $pp \rightarrow \tilde{\chi}_2^0 \tilde{\chi}_1^\pm \rightarrow \tilde{\chi}_1^0 Z^* \tilde{\chi}_1^0 W^{\pm*}$ obtained at ATLAS and CMS in the wino/bino(-) scenario, see our discussion in Sect. 3. As in the previous subsection, we only show the observed experimental limits, where for each Δm the stronger limit is indicated, including the 1σ theory uncertainties (with the same color coding as in Fig. 1). As before, we show in red the points that are in agreement with all constraints, as well as with both the LHC search limits from ATLAS and CMS. They are located at $m_{\tilde{\chi}_2^0} \gtrsim 225$ GeV (with the highest

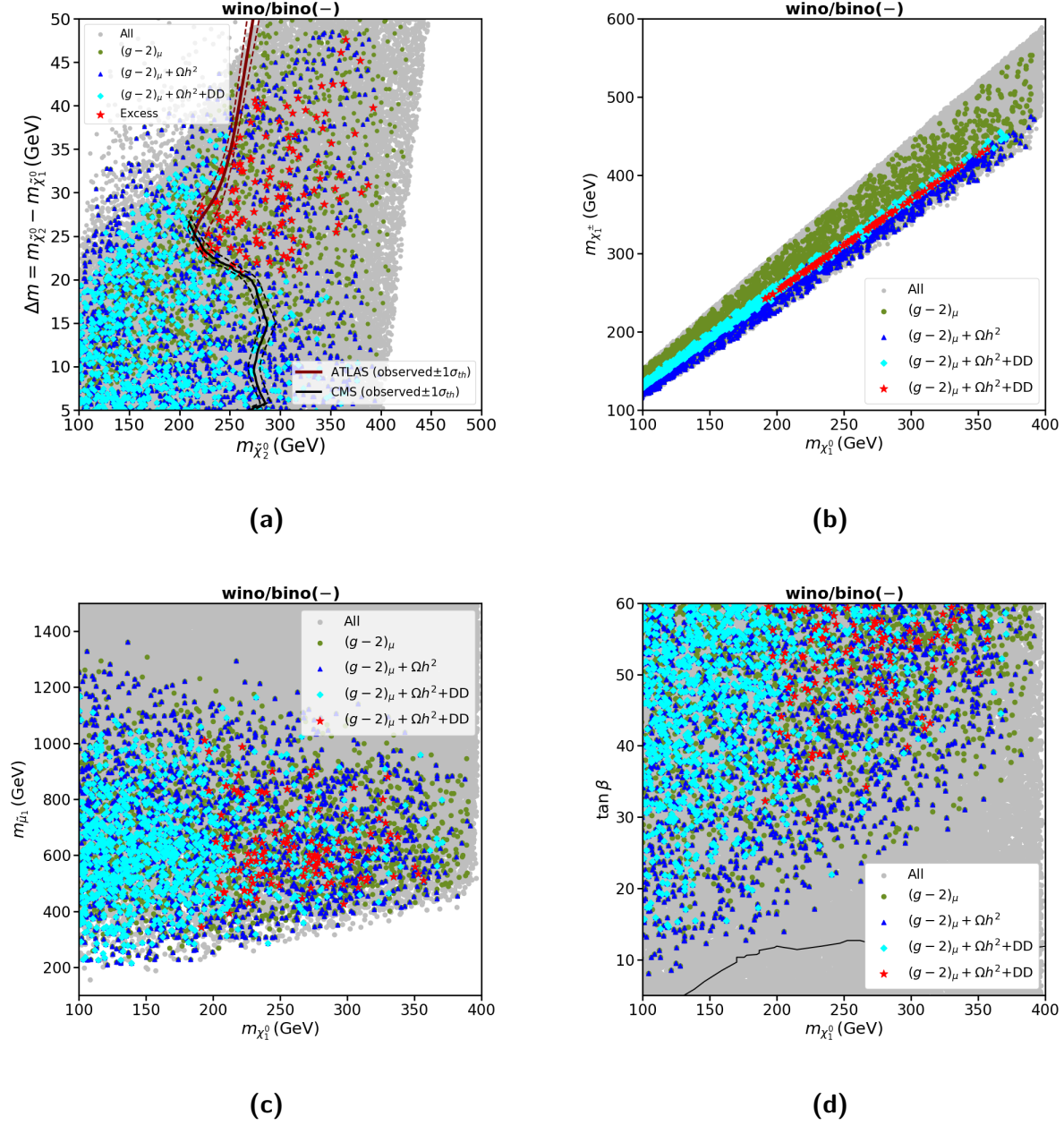


Figure 5: The results of our parameter scan in the wino/bino(-) case in the $m_{\tilde{\chi}_2^0}-\Delta m$ plane ($\Delta m = m_{\tilde{\chi}_2^0} - m_{\tilde{\chi}_1^0}$) (upper right), the $m_{\tilde{\chi}_1^\pm}-m_{\tilde{\chi}_2^0}$ plane (upper right), the $m_{\tilde{\chi}_1^0}-m_{\tilde{\mu}_1}$ plane (lower left), and the $m_{\tilde{\chi}_1^0}-\tan \beta$ plane (lower right).

value reaching up to ~ 400 GeV in our scan), and have a Δm of about 20 GeV to 45 GeV. Both excesses are well described by the red points.

The results for $m_{\tilde{\chi}_1^\pm} \sim m_{\tilde{\chi}_2^0}$ in our scan are shown in the $m_{\tilde{\chi}_1^0}-m_{\tilde{\chi}_1^\pm}$ plane in the upper right plot of Fig. 5. One can clearly observe that the DM constraints single out a small Δm

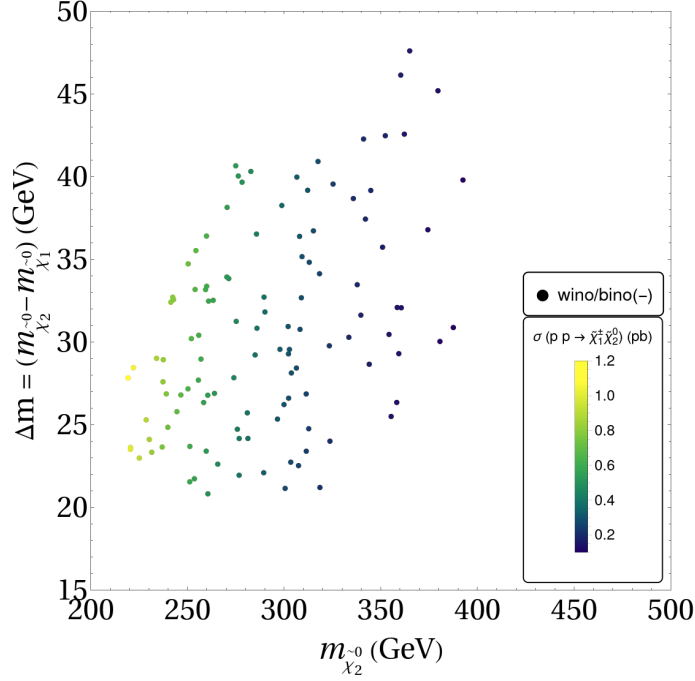


Figure 6: The results of our parameter scan in the wino/bino(-) scenario in the $m_{\tilde{\chi}_2^0} - \Delta m$ plane. Shown are only points allowed by all constraints. The color coding indicates the cross sections at the LHC at $\sqrt{s} = 13$ TeV.

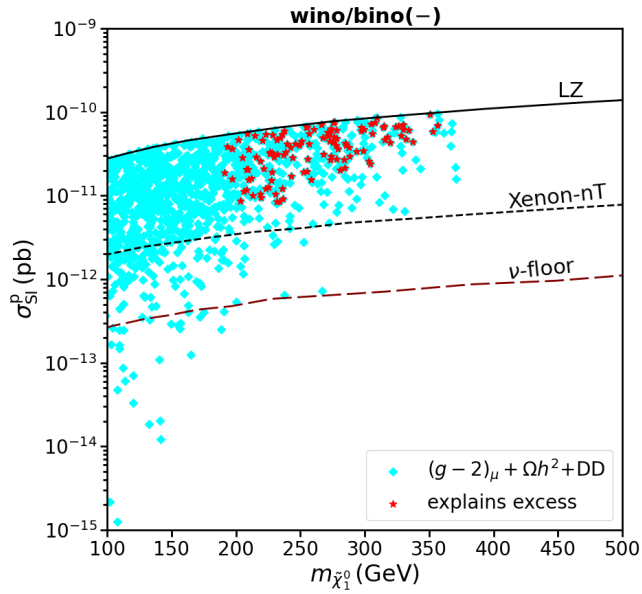


Figure 7: The results of our parameter scan in the wino/bino(-) scenario in the $m_{\tilde{\chi}_1^0} - \sigma_p^{SI}$ plane. Shown are only points allowed by DD limits (cyan and red).

in the wino/bino(-) scenario, corresponding to $\tilde{\chi}_1^\pm$ -coannihilation. The values range from $(m_{\tilde{\chi}_1^0}, m_{\tilde{\chi}_1^\pm}) \sim (200 \text{ GeV}, 220 \text{ GeV})$ up to $\sim (350 \text{ GeV}, 410 \text{ GeV})$.

The lower left plot of Fig. 5 shows the results in the $m_{\tilde{\chi}_1^0}$ - $m_{\tilde{\mu}_1}$ plane. We find a slightly larger spread in $m_{\tilde{\mu}_1}$ as compared to the wino/bino(+) scenario, $\sim 200 \text{ GeV} \lesssim m_{\tilde{\mu}_1} \lesssim 1000 \text{ GeV}$. Also in this scenario the range is driven by the $(g-2)_\mu$ requirement, see Eq. (1). However, as discussed above, the sleptons could be selected to be heavier, yielding a $\lesssim 2\sigma$ discrepancy for $(g-2)_\mu$, without changing the results of our analysis. In the lower right plot of Fig. 5 the results are shown in the $m_{\tilde{\chi}_1^0}$ - $\tan\beta$ plane. The same observations and conclusions as in the wino/bino(+) scenario hold.

The cross section for $pp \rightarrow \tilde{\chi}_2^0 \tilde{\chi}_1^\pm$ at the LHC at $\sqrt{s} = 13 \text{ TeV}$ in the wino/bino(-) scenarios is shown in the $m_{\tilde{\chi}_2^0}$ - Δm plane in Fig. 6 (evaluated the same way as for the wino/bino(+) case). The results are shown only for points passing all constraints (the red points in Fig. 5). The overall behavior of the cross section is as in the wino/bino(+) scenario, including the size of the largest and smallest values found. Also in this case, the values roughly agree with the cross sections needed to produce the observed excess in events (taking into account all uncertainties). On the other hand, this defines a target for the Run 3 of the LHC and beyond. The same conclusions as for the wino/bino(+) scenario hold.

Finally, also for the wino/bino(-) scenario we evaluate the DD prospects, which are presented in Fig. 7. In the $m_{\tilde{\chi}_1^0}$ - σ_p^{SI} plane we only show the points in agreement with the constraints up to the DM DD constraint in cyan, and the points that additionally describe all relevant LHC limits together with the ATLAS and CMS excesses in red (i.e. the same color coding as in Fig. 4). While the points fulfilling the DM constraints can reach well below the neutrino floor [108], the points selected by the ATLAS and CMS excesses are all well above the projected Xenon-nT/LZ limit. As a consequence, if the wino/bino(-) scenario is the correct description of the ATLAS and CMS excesses, we can expect these future DM experiments will see a positive DM signal in the coming years.

Concerning the prospects for future e^+e^- colliders, similar conclusions as for the wino/bino(+) scenario hold: all points of the wino/bino(-) scenario can be probed with a center-of-mass energy $\sqrt{s} \lesssim 800 \text{ GeV}$ (i.e. somewhat lower energies than in the wino/bino(+) scenario).

5.3 Preferred parameter ranges: higgsino(-)

The last scenario we analyze w.r.t. the reported excesses is the higgsino(-) scenario, see Eq. (7). For the higgsino DM scenario it is crucial to have $M_1 \times \mu < 0$. As shown in Ref. [18], for $M_1 \times \mu > 0$ the DD constraint cuts away $\Delta m \gtrsim 10 \text{ GeV}$, i.e. the region of interest. However, for $M_1 \times \mu < 0$ a cancellation of the h and H exchange in the DD cross section can occur. Consequently, going beyond our analysis in Ref. [18], we scanned this new parameter region according to Eq. (7). We note here that the $(g-2)_\mu$ constraint is not applied for this scenario, as discussed in Sect. 4. The results are shown in Fig. 8 the M_A - $\tan\beta$ plane (left) and in the M_1 - μ plane (right). The color coding is as in Figs. 2 and 5, with the exception that the LHC constraints (in particular concerning the excesses in the

$pp \rightarrow \tilde{\chi}_2^0 \tilde{\chi}_1^\pm$ search are not yet applied. However, the black line indicating the limits from the LHC searches for $pp \rightarrow H/A \rightarrow \tau^+ \tau^-$ (as taken from Ref. [86]) is included in the M_A - $\tan \beta$ plane, and the “surviving” points are marked in magenta. Furthermore, the gray shaded area indicates the parameter space with $M_A < 500$ GeV. Several “competing tendencies” can be observed in this plot. An effective cancellation of the h and H contributions to the DD cross section requires either very low M_A (where $M_A \sim M_H$ is naturally given in the MSSM) or very low $\tan \beta$, see Eq. (4). The low M_A points with $\tan \beta \gtrsim 2.5$, however, are cut away by the direct searches for the heavy Higgs bosons at the LHC, corresponding to the points shown in cyan. Only the magenta points survive both constraints. In the M_1 - μ plane (right plot of Fig. 8) the direct heavy Higgs-boson search cuts away the points with $M_1 \lesssim 1000$ GeV (cyan points).

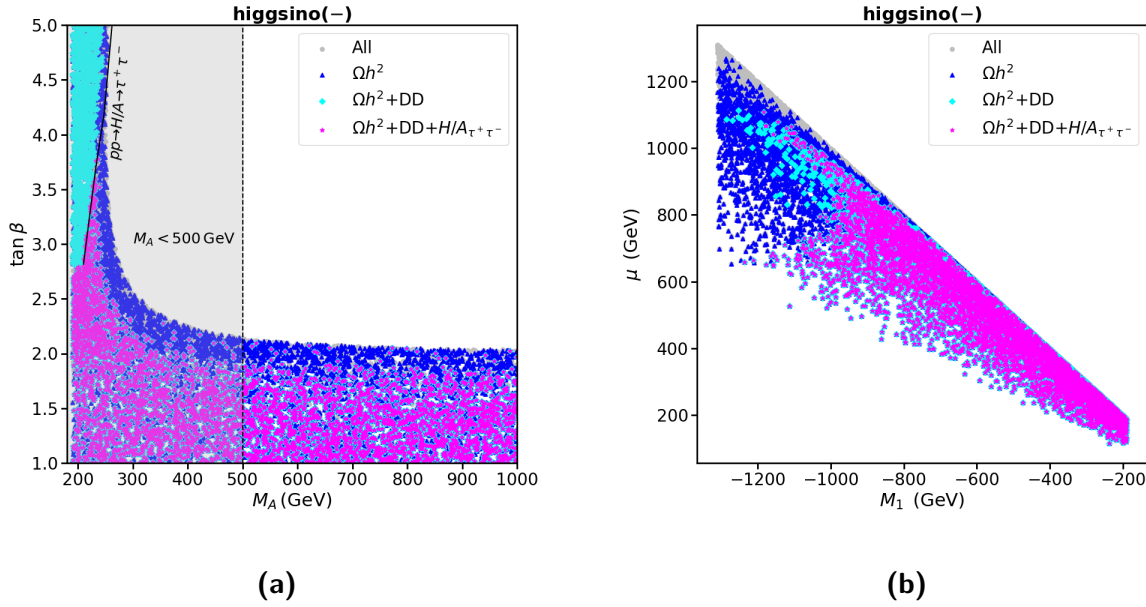


Figure 8: The input values of our parameter scans in the higgsino case in the M_A - $\tan \beta$ plane (left) and the M_1 - μ plane (right). For the color coding: see text.

The next constraint to be considered are the properties of the light \mathcal{CP} -even Higgs boson at ~ 125 GeV, which have to be in agreement with the LHC rate measurements, see our discussion in Sect. 3. The properties of the light \mathcal{CP} -even Higgs are driven by M_A and $\tan \beta$ at the tree-level. It has been shown (see, e.g., Ref. [86]) that for $M_A \gtrsim 500$ GeV the production and decay rates of the h are approaching their SM values and are thus consistent with the LHC measurements. Consequently, in the next step we discarded points with $M_A \lesssim 500$ GeV. We have indicated this additional constraint as the gray shaded area in the left plot of Fig. 8.

Our final results in the higgsino(-) scenario are shown in Fig. 9. In the $m_{\tilde{\chi}_2^0}$ - Δm plane (left plot) we compare the points found in our scan with the two main experimental limits for the search $pp \rightarrow \tilde{\chi}_2^0 \tilde{\chi}_1^\pm \rightarrow \tilde{\chi}_1^0 Z^* \tilde{\chi}_1^0 W^{\pm*}$ obtained at ATLAS and CMS in the higgsino(-) scenario, see our discussion in Sect. 3. As in the previous subsections, we only show the observed

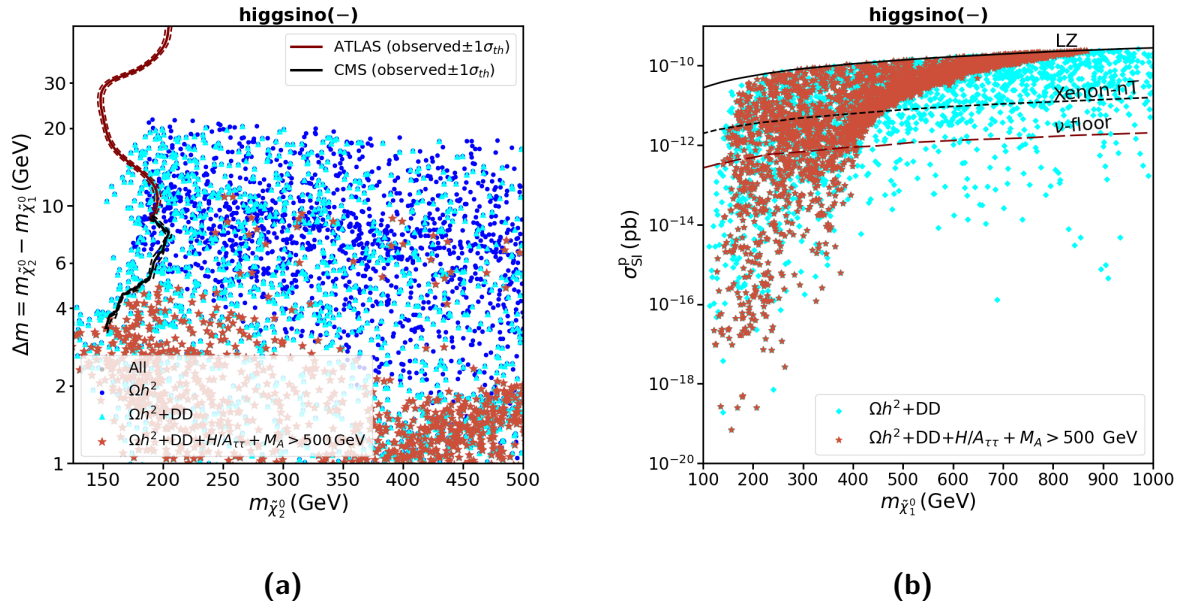


Figure 9: The results of our parameter scan in the higgsino(-) scenario in the $m_{\tilde{\chi}_2^0} - \Delta m$ plane ($\Delta m = m_{\tilde{\chi}_2^0} - m_{\tilde{\chi}_1^0}$) (left) and the SI direct detection cross section as a function of the $\tilde{\chi}_1^0$ mass (right). For the color coding: see text.

experimental limits, where for each Δm the stronger limit is indicated, including the 1σ theory uncertainties (with the same color coding as in Fig. 1). Instead of red points passing all constraints, here we mark in brown the points that additionally satisfy $M_A > 500$ GeV. The brown points all have $\Delta m \lesssim 10$ GeV. Consequently, they do not present a good description of the observed excesses, and we conclude that the higgsino DM scenario within the MSSM cannot be regarded as an explanation².

For the sake of completeness, we show in the right plot of Fig. 9 the $m_{\tilde{\chi}_1^0} - \sigma_p^{\text{SI}}$ plane, focusing on the points in agreement with the DM constraints. The color coding is the same as in the left plot (but only cyan and brown are shown). One can observe that the brown points could be covered for $m_{\tilde{\chi}_2^0} \gtrsim 400$ GeV by the next round of Xenon-based DD experiments. Lighter masses, which are more easily accessible at the HL-LHC or possible future e^+e^- colliders are found also at lower cross sections, going even below the neutrino floor. While this complementary coverage of the allowed points in the higgsino(-) scenario hold (complementing the higgsino(+) case studied in Ref. [22]), it does not yield a good description of the ATLAS and CMS excesses, as discussed above.

²The situation may change in the next-to-minimal MSSM (NMSSM) [109].

5.4 Photonic decays

In this subsection we conclude with comments on the assumption of $\text{BR}(\tilde{\chi}_2^0 \rightarrow \tilde{\chi}_1^0 Z)$ as made in the simplified model analyses of ATLAS and CMS. While in principle the decay $\tilde{\chi}_2^0 \rightarrow \tilde{\chi}_1^0 h$ can be relevant [110], this decay is strongly suppressed in the parameter space with compressed spectra. However, the loop-induced decay $\tilde{\chi}_2^0 \rightarrow \tilde{\chi}_1^0 \gamma$ can also be relevant, not suffering from a phase space suppression³. In order to assess the relevance of this decay mode we have evaluated $\Gamma(\tilde{\chi}_2^0 \rightarrow \tilde{\chi}_1^0 \gamma)$ with the help of the code `SDECAY-v1.5a` [98] for the points passing all constraints (the “red/brown points”). Since $\tilde{\chi}_1^0 \gamma$ is the only decay mode competing with $\tilde{\chi}_1^0 Z^*$, we show $\text{BR}(\tilde{\chi}_2^0 \rightarrow \tilde{\chi}_1^0 \gamma)$ for the three scenarios in Fig. 10 as a function of $\Delta m := m_{\tilde{\chi}_2^0} - m_{\tilde{\chi}_1^0}$. In the wino/bino(+) (wino/bino(-)) scenario values between zero going up to 20(40)% are reached, where the largest BRs are found for the smallest Δm . However, the Δm corresponding to the largest observed excess in the $pp \rightarrow \tilde{\chi}_2^0 \tilde{\chi}_1^\pm$ searches found in our scan is higher by a few GeV than the lowest possible Δm . For these slightly higher Δm somewhat smaller values of $\text{BR}(\tilde{\chi}_2^0 \rightarrow \tilde{\chi}_1^0 \gamma)$ are obtained. On the other hand, since for each Δm also values of $\text{BR}(\tilde{\chi}_2^0 \rightarrow \tilde{\chi}_1^0 \gamma)$ close to zero are found, we conclude that this decay, lowering the real $\text{BR}(\tilde{\chi}_2^0 \rightarrow \tilde{\chi}_1^0 Z^*)$, does not endanger the wino/bino(+) or wino/bino(-) scenarios as a possible explanation of the observed excesses. For the higgsino(-) scenario we find BRs going to zero for increasing Δm , i.e. in the potentially relevant parameter space with sufficiently large Δm (which is not reached due to our requirement of $M_A > 500$ GeV) the decay $\tilde{\chi}_2^0 \rightarrow \tilde{\chi}_1^0 \gamma$ does not play a relevant role.

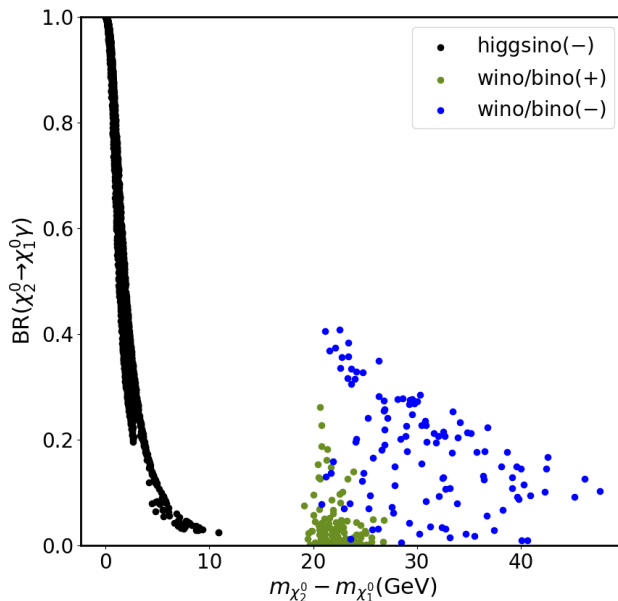


Figure 10: $\text{BR}(\tilde{\chi}_2^0 \rightarrow \tilde{\chi}_1^0 \gamma)$ as a function of Δm in the three scenarios (see text).

³The relevance of this decay mode has been discussed previously in the context of bino-wino coannihilation in Refs. [78, 111].

6 Conclusions

The EW sector of the MSSM, consisting of four neutralinos, $\tilde{\chi}_{1,2,3,4}^0$, two charginos, $\tilde{\chi}_{1,2}^\pm$, as well as the SUSY partners of the SM leptons, can account for a variety of experimental data. In particular, the LSP, assumed to be the lightest neutralino, $\tilde{\chi}_1^0$, as a DM candidate is in good agreement with the observed limits on the DM content of the universe, as well as with negative results from DD experiments.

At the LHC, a wide range of experimental searches has been designed to look for the production and decays of the EWinos and sleptons in various final states. Some of the most stringent constraints on the EW MSSM parameter space can be obtained from the searches looking for the production of a heavier neutralino and the lightest chargino, $pp \rightarrow \tilde{\chi}_2^0, \tilde{\chi}_1^\pm \rightarrow \tilde{\chi}_1^0 Z^{(*)} \tilde{\chi}_1^0 W^{\pm(*)}$. The targeted final states contain two or three leptons accompanied by a substantial amount of \cancel{E}_T . These searches become particularly challenging in the region of parameter space where the mass difference between the initial and the final state EWinos become small, making the visible final state leptons, to be rather soft. The ATLAS and CMS collaborations are actively searching for the EWinos in this “compressed spectra” region in soft dilepton and \cancel{E}_T final states. Interestingly, recent searches for the “golden channel”, $pp \rightarrow \tilde{\chi}_2^0, \tilde{\chi}_1^\pm \rightarrow \tilde{\chi}_1^0 Z^{(*)} \tilde{\chi}_1^0 W^{\pm(*)}$ show consistent excesses between ATLAS and CMS in the soft 2/3 lepton plus missing energy [10, 11], and combined 2/3 leptons plus missing energy [12, 13]. The mono-jet searches [14–16] also report excesses in a similar mass region. These searches assume simplified model scenarios with $m_{\tilde{\chi}_2^0} \approx m_{\tilde{\chi}_1^\pm}$ and $\Delta m := m_{\tilde{\chi}_2^0} - m_{\tilde{\chi}_1^0} \approx 20$ GeV. The sleptons are assumed to be heavier and not taking part in the decays of the initially produced EWinos. Naturally, it seems interesting to identify the underlying parameter space of the EW MSSM and analyze the associated properties of the EWinos that can give rise to such excesses at the LHC.

Based on previous analyses [17–22], taking into account the DM and DD constraints, two scenarios were identified that can potentially give rise to the mass configuration in which the excesses in the LHC searches have been observed. (i) wino/bino DM with $\tilde{\chi}_1^\pm$ -coannihilation ($|M_1| \lesssim |M_2|$), (ii) higgsino DM ($|\mu| < |M_1|, |M_2|$). In this paper we analyzed these two MSSM scenarios at the EW scale w.r.t. the consistent experimental excesses in the search $pp \rightarrow \tilde{\chi}_2^0, \tilde{\chi}_1^\pm \rightarrow \tilde{\chi}_1^0 Z^{(*)} \tilde{\chi}_1^0 W^{\pm(*)}$, taking into account all other relevant experimental constraints. We assumed $\mu, M_2 > 0$ throughout our analysis, but allow for positive and negative M_1 . This is in contrast to Refs. [17–22], where all parameters were assumed to be positive. Allowing for $\mu \times M_1 < 0$, this can yield lower DM DD rates, and can have important consequences for the chargino/neutralino production cross sections at the LHC. In our initial parameter scan also a discrepancy in a_μ at the 5σ level was assumed, whereas recent lattice calculations favor a discrepancy at the $\lesssim 2\sigma$ level. However, as mentioned above, the searches for EWinos require the sleptons to be heavier than the lighter neutralinos and charginos, so that they do not play any role in the searches for the EWinos. Sufficiently higher values for the slepton masses can easily decrease the SUSY contribution to a_μ to yield the $\lesssim 2\sigma$ discrepancy as suggested by the lattice calculations.

In the case of wino/bino DM with $\tilde{\chi}_1^\pm$ -coannihilation we analyzed two scenarios, wino/bino(+) with $M_1 \times \mu > 0$, and wino/bino(−) with $M_1 \times \mu < 0$. In the wino/bino(+) scenario the excesses

can be described by parameter points located at $m_{\tilde{\chi}_2^0} \gtrsim 250$ GeV (with the highest value reaching up to ~ 450 GeV in our scan), and have a Δm of about 18 GeV \dots 25 GeV. While the ATLAS excess is well described, the CMS excess would prefer slightly higher values of Δm (minding the experimental uncertainties in Δm). The cross section for $pp \rightarrow \tilde{\chi}_2^0 \tilde{\chi}_1^\pm$ at the LHC at $\sqrt{s} = 13$ TeV has been calculated. The smallest EWino masses yield production cross sections of ~ 1 pb, going down to ~ 0.2 pb for the highest mass values. This roughly agrees with the cross sections needed to produce the observed excess in events and sets a target for the Run 3 of the LHC and beyond. We also evaluated the future prospects for DD experiments. All “preferred” points are above the projected Xenon-nT/LZ limit. Hence, the future DM DD experiments will put this scenario under test and can play a complimentary role to future LHC searches. Concerning the prospects at future e^+e^- collider experiments, such as ILC or CLIC, in the wino/bino(+) scenario a center-of-mass energy of $\sqrt{s} \lesssim 1000$ GeV is sufficient to conclusively test this scenario.

The results in the wino/bino(-) scenario are very similar to the ones in the wino/bino(+) case. The points fulfilling all constraints and yielding a good description of the excesses are located at $m_{\tilde{\chi}_2^0} \gtrsim 225$ GeV (with the highest value reaching up to ~ 400 GeV in our scan), and have a Δm of about 20 GeV to 45 GeV. Both excesses are described equally well. The cross section for $pp \rightarrow \tilde{\chi}_2^0 \tilde{\chi}_1^\pm$ at the LHC at $\sqrt{s} = 13$ TeV in the wino/bino(-) scenarios reaches the same values as in the wino/bino(+) scenario, yielding the same conclusions. Also the DD prospects are very similar. While the points fulfilling the DM constraints can reach well below the neutrino floor, the points selected by the ATLAS and CMS excesses are all well above the projected Xenon-nT/LZ limit. Akin to the previous case, this scenario will also be an important candidate to future DM DD searches with interesting perspectives for a positive signal. Concerning the prospects for future e^+e^- colliders, the wino/bino(-) scenario can be probed with a center-of-mass energy $\sqrt{s} \lesssim 800$ GeV (i.e. somewhat lower energies than in the wino/bino(+) scenario).

Finally, in the higgsino(-) scenario several “competing tendencies” were observed. An effective cancellation of the h and H contributions to the DD cross section requires either very low M_A or very low $\tan \beta$. The low M_A points with $\tan \beta \gtrsim 2.5$, however, are cut away by the direct searches for the heavy Higgs bosons at the LHC. Points below $M_A \sim 500$ GeV are excluded by the LHC Higgs-boson rate measurements. All points fulfilling these constraints have $\Delta m \lesssim 10$ GeV. Consequently, this do not yield a good description of the observed excesses, and we conclude that the higgsino DM scenario within the MSSM cannot be regarded as an explanation.

For the first time, ATLAS and CMS see excesses in the search for SUSY particles that are in agreement with each other. These excesses are observed in three different searches in the processes $pp \rightarrow \tilde{\chi}_2^0 \tilde{\chi}_1^\pm \rightarrow \tilde{\chi}_1^0 Z^* \tilde{\chi}_1^0 W^*$: $2l$ and \cancel{E}_T , $3l$ and \cancel{E}_T as well as the mono-jet searches. The masses would be $m_{\tilde{\chi}_2^0} \approx m_{\tilde{\chi}_1^\pm} \gtrsim 250$ GeV and $m_{\tilde{\chi}_2^0} - m_{\tilde{\chi}_1^0} \approx 20$ GeV. While each search and experiment individually is not significant by itself, the occurrence of excesses in multiple search channels, observed by both ATLAS and CMS, gives rise to the hope that finally a glimpse of BSM physics has been observed. We are eagerly awaiting the corresponding upcoming Run 3 results.

Acknowledgments

We thank J. Montejo Berlingen for helpful discussions. I.S. acknowledges support from DST-INSPIRE, India, under grant no. IFA21-PH272. The work of S.H. has received financial support from the grant PID2019-110058GB-C21 funded by MCIN/AEI/10.13039/501100011033 and by “ERDF A way of making Europe”, and in part by the grant IFT Centro de Excelencia Severo Ochoa CEX2020-001007-S funded by MCIN/AEI/10.13039/501100011033. S.H. also acknowledges support from Grant PID2022-142545NB-C21 funded by MCIN/AEI/10.13039/501100011033/ FEDER, UE. We acknowledge the use of the IFT Hydra computation cluster for a part of our numerical analysis.

References

- [1] H. Nilles, *Phys. Rept.* **110** (1984) 1.
- [2] R. Barbieri, *Riv. Nuovo Cim.* **11** (1988) 1.
- [3] H. Haber, G. Kane, *Phys. Rept.* **117** (1985) 75.
- [4] J. Gunion, H. Haber, *Nucl. Phys.* **B 272** (1986) 1.
- [5] S. Heinemeyer and C. Muñoz, *Universe* **8** (2022) no.8, 427.
- [6] H. Goldberg, *Phys. Rev. Lett.* **50** (1983) 1419.
- [7] J. Ellis, J. Hagelin, D. Nanopoulos, K. Olive, M. Srednicki, *Nucl. Phys.* **B 238** (1984) 453.
- [8] See: <https://twiki.cern.ch/twiki/bin/view/AtlasPublic/SupersymmetryPublicResults> .
- [9] See: <https://twiki.cern.ch/twiki/bin/view/CMSPublic/PhysicsResultsSUS> .
- [10] G. Aad *et al.* [ATLAS], *Phys. Rev.* **D 101** (2020) no.5, 052005 [[arXiv:1911.12606](https://arxiv.org/abs/1911.12606) [hep-ex]].
- [11] A. Tumasyan *et al.* [CMS], *JHEP* **04** (2022), 091 [[arXiv:2111.06296](https://arxiv.org/abs/2111.06296) [hep-ex]].
- [12] G. Aad *et al.* [ATLAS], *Eur. Phys. J.* **C 81** (2021) no.12, 1118 [[arXiv:2106.01676](https://arxiv.org/abs/2106.01676) [hep-ex]].
- [13] [CMS], CMS-PAS-SUS-21-008.
- [14] D. Agin, B. Fuks, M. D. Goodsell and T. Murphy, [[arXiv:2311.17149](https://arxiv.org/abs/2311.17149) [hep-ph]].
- [15] G. Aad *et al.* [ATLAS], *Phys. Rev.* **D 103** (2021) no.11, 112006 [[arXiv:2102.10874](https://arxiv.org/abs/2102.10874) [hep-ex]].
- [16] A. Tumasyan *et al.* [CMS], *JHEP* **11** (2021), 153 [[arXiv:2107.13021](https://arxiv.org/abs/2107.13021) [hep-ex]].

- [17] M. Chakraborti, S. Heinemeyer and I. Saha, *Eur. Phys. J. C* **80** (2020) 10, 984 [[arXiv:2006.15157](#) [hep-ph]].
- [18] M. Chakraborti, S. Heinemeyer and I. Saha, *Eur. Phys. J. C* **81** (2021) no.12, 1069 [[arXiv:2103.13403](#) [hep-ph]].
- [19] M. Chakraborti, S. Heinemeyer and I. Saha, *Eur. Phys. J. C* **81** (2021) no.12, 1114 [[arXiv:2104.03287](#) [hep-ph]].
- [20] M. Chakraborti, S. Heinemeyer, I. Saha and C. Schappacher, *Eur. Phys. J. C* **82** (2022) no.5, 483 [[arXiv:2112.01389](#) [hep-ph]].
- [21] E. Bagnaschi, M. Chakraborti, S. Heinemeyer, I. Saha and G. Weiglein, *Eur. Phys. J. C* **82** (2022) no.5, 474 [[arXiv:2203.15710](#) [hep-ph]].
- [22] M. Chakraborti, S. Heinemeyer and I. Saha, *Eur. Phys. J. C* **84** (2024) no.2, 165 [[arXiv:2308.05723](#) [hep-ph]].
- [23] N. Aghanim *et al.* [Planck Collaboration], *Astron. Astrophys.* **641** (2020), A6 [erratum: *Astron. Astrophys.* **652** (2021), C4] [[arXiv:1807.06209](#) [astro-ph.CO]].
- [24] E. Aprile *et al.* [XENON Collaboration], *Phys. Rev. Lett.* **121** (2018) no.11, 111302 [[arXiv:1805.12562](#) [astro-ph.CO]].
- [25] D. S. Akerib *et al.* [LUX Collaboration], *Phys. Rev. Lett.* **118** (2017) no.2, 021303 [[arXiv:1608.07648](#) [astro-ph.CO]].
- [26] X. Cui *et al.* [PandaX-II Collaboration], *Phys. Rev. Lett.* **119** (2017) no.18, 181302 [[arXiv:1708.06917](#) [astro-ph.CO]].
- [27] D. P. Aguillard *et al.* [Muon g-2], *Phys. Rev. Lett.* **131** (2023) no.16, 161802 [[arXiv:2308.06230](#) [hep-ex]].
- [28] B. Abi *et al.* [Muon g-2], *Phys. Rev. Lett.* **126** (2021) no.14, 141801 [[arXiv:2104.03281](#) [hep-ex]].
- [29] G. W. Bennett *et al.* [Muon g-2 Collaboration], *Phys. Rev. D* **73** (2006) 072003 [[hep-ex/0602035](#)].
- [30] T. Aoyama *et al.*, *Phys. Rept.* **887** (2020), 1-166 [[arXiv:2006.04822](#) [hep-ph]].
- [31] T. Aoyama, M. Hayakawa, T. Kinoshita and M. Nio, *Phys. Rev. Lett.* **109** (2012), 111808 [[arXiv:1205.5370](#) [hep-ph]].
- [32] T. Aoyama, T. Kinoshita and M. Nio, *Atoms* **7** (2019) no.1, 28.
- [33] A. Czarnecki, W. J. Marciano and A. Vainshtein, *Phys. Rev. D* **67** (2003), 073006 [[arXiv:hep-ph/0212229](#) [hep-ph]].
- [34] C. Gnendiger, D. Stöckinger and H. Stöckinger-Kim, *Phys. Rev. D* **88** (2013), 053005 [[arXiv:1306.5546](#) [hep-ph]].

- [35] M. Davier, A. Hoecker, B. Malaescu and Z. Zhang, *Eur. Phys. J. C* **77** (2017) no.12, 827 [[arXiv:1706.09436](#) [hep-ph]].
- [36] A. Keshavarzi, D. Nomura and T. Teubner, *Phys. Rev. D* **97** (2018) no.11, 114025 [[arXiv:1802.02995](#) [hep-ph]].
- [37] G. Colangelo, M. Hoferichter and P. Stoffer, *JHEP* **02** (2019), 006 [[arXiv:1810.00007](#) [hep-ph]].
- [38] M. Hoferichter, B. L. Hoid and B. Kubis, *JHEP* **08** (2019), 137 [[arXiv:1907.01556](#) [hep-ph]].
- [39] M. Davier, A. Hoecker, B. Malaescu and Z. Zhang, *Eur. Phys. J. C* **80** (2020) no.3, 241 [erratum: *Eur. Phys. J. C* **80** (2020) no.5, 410] [[arXiv:1908.00921](#) [hep-ph]].
- [40] A. Keshavarzi, D. Nomura and T. Teubner, *Phys. Rev. D* **101**, no.1, 014029 (2020) [[arXiv:1911.00367](#) [hep-ph]].
- [41] A. Kurz, T. Liu, P. Marquard and M. Steinhauser, *Phys. Lett. B* **734** (2014), 144-147 [[arXiv:1403.6400](#) [hep-ph]].
- [42] K. Melnikov and A. Vainshtein, *Phys. Rev. D* **70** (2004), 113006 [[arXiv:hep-ph/0312226](#) [hep-ph]].
- [43] P. Masjuan and P. Sanchez-Puertas, *Phys. Rev. D* **95** (2017) no.5, 054026 [[arXiv:1701.05829](#) [hep-ph]].
- [44] G. Colangelo, M. Hoferichter, M. Procura and P. Stoffer, *JHEP* **04** (2017), 161 [[arXiv:1702.07347](#) [hep-ph]].
- [45] M. Hoferichter, B. L. Hoid, B. Kubis, S. Leupold and S. P. Schneider, *JHEP* **10** (2018), 141 [[arXiv:1808.04823](#) [hep-ph]].
- [46] A. Gérardin, H. B. Meyer and A. Nyffeler, *Phys. Rev. D* **100** (2019) no.3, 034520 [[arXiv:1903.09471](#) [hep-lat]].
- [47] J. Bijnens, N. Hermansson-Truedsson and A. Rodríguez-Sánchez, *Phys. Lett. B* **798** (2019), 134994 [[arXiv:1908.03331](#) [hep-ph]].
- [48] G. Colangelo, F. Hagelstein, M. Hoferichter, L. Laub and P. Stoffer, *JHEP* **03** (2020), 101 [[arXiv:1910.13432](#) [hep-ph]].
- [49] T. Blum, N. Christ, M. Hayakawa, T. Izubuchi, L. Jin, C. Jung and C. Lehner, *Phys. Rev. Lett.* **124** (2020) no.13, 132002 [[arXiv:1911.08123](#) [hep-lat]].
- [50] G. Colangelo, M. Hoferichter, A. Nyffeler, M. Passera and P. Stoffer, *Phys. Lett. B* **735** (2014), 90-91 [[arXiv:1403.7512](#) [hep-ph]].
- [51] S. Borsanyi *et al.*, *Nature* **593** (2021) no.7857, 51-55 [[arXiv:2002.12347](#) [hep-lat]].

- [52] P. Huang and C. E. M. Wagner, *Phys. Rev. D* **90** (2014) no.1, 015018 [[arXiv:1404.0392](#) [hep-ph]].
- [53] S. Baum, M. Carena, N. R. Shah and C. E. M. Wagner, *JHEP* **01** (2022), 025 [[arXiv:2104.03302](#) [hep-ph]].
- [54] E. Bagnaschi *et al.*, *Eur. Phys. J. C* **78** (2018) no.3, 256 [[arXiv:1710.11091](#) [hep-ph]].
- [55] P. Slavich, S. Heinemeyer (eds.), E. Bagnaschi *et al.*, *Eur. Phys. J. C* **81** (2021) no.5, 450 [[arXiv:2012.15629](#) [hep-ph]].
- [56] J. L. Lopez, D. V. Nanopoulos and X. Wang, *Phys. Rev. D* **49** (1994), 366-372 [[arXiv:hep-ph/9308336](#) [hep-ph]].
- [57] U. Chattopadhyay and P. Nath, *Phys. Rev. D* **53** (1996), 1648-1657 [[arXiv:hep-ph/9507386](#) [hep-ph]].
- [58] U. Chattopadhyay, D. K. Ghosh and S. Roy, *Phys. Rev. D* **62** (2000), 115001 [[arXiv:hep-ph/0006049](#) [hep-ph]].
- [59] K. Kowalska, L. Roszkowski, E. M. Sessolo and A. J. Williams, *JHEP* **06** (2015), 020 [[arXiv:1503.08219](#) [hep-ph]].
- [60] M. Cè *et al.* *Phys. Rev. D* **106** (2022) no.11, 114502 [[arXiv:2206.06582](#) [hep-lat]].
- [61] C. Alexandrou *et al.* [Extended Twisted Mass], *Phys. Rev. D* **107** (2023) no.7, 074506 [[arXiv:2206.15084](#) [hep-lat]].
- [62] P. von Weitershausen, M. Schafer, H. Stöckinger-Kim and D. Stöckinger, *Phys. Rev. D* **81** (2010), 093004 [[arXiv:1003.5820](#) [hep-ph]].
- [63] H. Fargnoli, C. Gnendiger, S. Paßehr, D. Stöckinger and H. Stöckinger-Kim, *JHEP* **1402** (2014), 070 [[arXiv:1311.1775](#) [hep-ph]].
- [64] M. Bach, J. h. Park, D. Stöckinger and H. Stöckinger-Kim, *JHEP* **1510** (2015), 026 [[arXiv:1504.05500](#) [hep-ph]].
- [65] S. Heinemeyer, D. Stöckinger and G. Weiglein, *Nucl. Phys. B* **690** (2004), 62-80 [[arXiv:hep-ph/0312264](#) [hep-ph]].
- [66] S. Heinemeyer, D. Stöckinger and G. Weiglein, *Nucl. Phys. B* **699** (2004), 103-123 [[arXiv:hep-ph/0405255](#) [hep-ph]].
- [67] P. Athron *et al.*, *Eur. Phys. J. C* **76** (2016) no.2, 62 [[arXiv:1510.08071](#) [hep-ph]].
- [68] J. F. Gunion, H. E. Haber and M. Sher, *Nucl. Phys. B* **306** (1988), 1-13.
- [69] J. A. Casas, A. Lleyda and C. Munoz, *Nucl. Phys. B* **471** (1996), 3-58 [[arXiv:hep-ph/9507294](#) [hep-ph]].
- [70] U. Chattopadhyay and A. Dey, *JHEP* **11** (2014), 161 [[arXiv:1409.0611](#) [hep-ph]].

- [71] W. G. Hollik, G. Weiglein and J. Wittbrodt, *JHEP* **03** (2019), 109 [[arXiv:1812.04644](#) [hep-ph]].
- [72] P. M. Ferreira, M. Mühlleitner, R. Santos, G. Weiglein and J. Wittbrodt, *JHEP* **09** (2019), 006 [[arXiv:1905.10234](#) [hep-ph]].
- [73] G. Belanger, F. Boudjema, A. Pukhov and A. Semenov, *Comput. Phys. Commun.* **149** (2002), 103-120 [[arXiv:hep-ph/0112278](#) [hep-ph]].
- [74] G. Belanger, F. Boudjema, A. Pukhov and A. Semenov, *Comput. Phys. Commun.* **176** (2007), 367-382 [[arXiv:hep-ph/0607059](#) [hep-ph]].
- [75] G. Belanger, F. Boudjema, A. Pukhov and A. Semenov, *Comput. Phys. Commun.* **177** (2007), 894-895.
- [76] G. Belanger, F. Boudjema, A. Pukhov and A. Semenov, [arXiv:1305.0237](#) [hep-ph].
- [77] J. Aalbers *et al.* [LZ], *Phys. Rev. Lett.* **131** (2023) no.4, 041002 [[arXiv:2207.03764](#) [hep-ex]].
- [78] S. Baum, M. Carena, T. Ou, D. Rocha, N. R. Shah and C. E. M. Wagner, *JHEP* **11** (2023), 037 [[arXiv:2303.01523](#) [hep-ph]].
- [79] T. R. Slatyer, [[arXiv:1710.05137](#) [hep-ph]].
- [80] A. Hryczuk, K. Jodlowski, E. Moulin, L. Rinchuso, L. Roszkowski, E. M. Sessolo and S. Trojanowski, *JHEP* **10** (2019), 043 [[arXiv:1905.00315](#) [hep-ph]].
- [81] L. Rinchuso, O. Macias, E. Moulin, N. L. Rodd and T. R. Slatyer, *Phys. Rev. D* **103** (2021) no.2, 023011 [[arXiv:2008.00692](#) [astro-ph.HE]].
- [82] R. T. Co, B. Sheff and J. D. Wells, *Phys. Rev. D* **105** (2022) no.3, 035012 [[arXiv:2105.12142](#) [hep-ph]].
- [83] A. McDaniel, M. Ajello, C. M. Karwin, M. Di Mauro, A. Drlica-Wagner and M. Sánchez-Conde, [[arXiv:2311.04982](#) [astro-ph.HE]].
- [84] M. Ackermann *et al.* [Fermi-LAT], *Phys. Rev. Lett.* **115** (2015) no.23, 231301 [[arXiv:1503.02641](#) [astro-ph.HE]].
- [85] G. Aad *et al.* [ATLAS and CMS], *Phys. Rev. Lett.* **114** (2015), 191803 [[arXiv:1503.07589](#) [hep-ex]].
- [86] E. Bagnaschi *et al.* *Eur. Phys. J. C* **79** (2019) no.7, 617 [[arXiv:1808.07542](#) [hep-ph]].
- [87] H. Bahl, P. Bechtle, S. Heinemeyer, S. Liebler, T. Stefaniak and G. Weiglein, *Eur. Phys. J. C* **80** (2020) no.10, 916 [[arXiv:2005.14536](#) [hep-ph]].
- [88] T. Enomoto and R. Watanabe, *JHEP* **1605** (2016) 002 [[arXiv:1511.05066](#) [hep-ph]].

- [89] A. Arbey, F. Mahmoudi, O. Stål and T. Stefaniak, *Eur. Phys. J. C* **78** (2018) no.3, 182 [[arXiv:1706.07414](#) [hep-ph]].
- [90] J. Haller, A. Hoecker, R. Kogler, K. Mönig, T. Peiffer and J. Stelzer, *Eur. Phys. J. C* **78** (2018) no.8, 675 [[arXiv:1803.01853](#) [hep-ph]].
- [91] G. Aad *et al.* [ATLAS Collaboration], *Eur. Phys. J. C* **80** (2020) no.2, 123 [[arXiv:1908.08215](#) [hep-ex]].
- [92] M. Drees, H. Dreiner, D. Schmeier, J. Tattersall and J. S. Kim, *Comput. Phys. Commun.* **187** (2015), 227-265 [[arXiv:1312.2591](#) [hep-ph]].
- [93] J. S. Kim, D. Schmeier, J. Tattersall and K. Rolbiecki, *Comput. Phys. Commun.* **196** (2015), 535-562 [[arXiv:1503.01123](#) [hep-ph]].
- [94] D. Dercks, N. Desai, J. S. Kim, K. Rolbiecki, J. Tattersall and T. Weber, *Comput. Phys. Commun.* **221** (2017), 383-418 [[arXiv:1611.09856](#) [hep-ph]].
- [95] A. Djouadi, J. L. Kneur and G. Moultaka, *Comput. Phys. Commun.* **176** (2007) 426 [[hep-ph/0211331](#)].
- [96] J. L. Kneur, G. Moultaka, M. Ughetto, D. Zerwas and A. Djouadi, *Comput. Phys. Commun.* **291** (2023), 108805 [[arXiv:2211.16956](#) [hep-ph]].
- [97] Joint LEP2 SUSY Working Group, the ALEPH, DELPHI, L3 and OPAL Collaborations, see: <http://lepsusy.web.cern.ch/lepsusy/>.
- [98] M. Mühlleitner, A. Djouadi and Y. Mambrini, *Comput. Phys. Commun.* **168** (2005) 46 [[hep-ph/0311167](#)].
- [99] B. Fuks, M. Klasen, D. R. Lamprea and M. Rothering, *Eur. Phys. J. C* **73** (2013), 2480 [[arXiv:1304.0790](#) [hep-ph]].
- [100] G. Bozzi, B. Fuks and M. Klasen, *Phys. Rev. D* **74** (2006), 015001 [[arXiv:hep-ph/0603074](#) [hep-ph]].
- [101] G. Bozzi, B. Fuks and M. Klasen, *Nucl. Phys. B* **777** (2007), 157-181 [[arXiv:hep-ph/0701202](#) [hep-ph]].
- [102] J. Debove, B. Fuks and M. Klasen, *Phys. Lett. B* **688** (2010), 208-211 [[arXiv:0907.1105](#) [hep-ph]].
- [103] J. Debove, B. Fuks and M. Klasen, *Nucl. Phys. B* **842** (2011), 51-85 [[arXiv:1005.2909](#) [hep-ph]].
- [104] E. Aprile *et al.* [XENON], *JCAP* **11** (2020), 031 [[arXiv:2007.08796](#) [physics.ins-det]].
- [105] D. S. Akerib *et al.* [LUX-ZEPLIN], *Phys. Rev. D* **101** (2020) no.5, 052002 [[arXiv:1802.06039](#) [astro-ph.IM]].
- [106] R. K. Ellis *et al.* [[arXiv:1910.11775](#) [hep-ex]].

- [107] M. Berggren, [[arXiv:2003.12391](#) [hep-ph]].
- [108] F. Ruppin, J. Billard, E. Figueroa-Feliciano and L. Strigari, *Phys. Rev. D* **90** (2014) no.8, 083510 [[arXiv:1408.3581](#) [hep-ph]].
- [109] M. Badziak, M. Olechowski and P. Szczerbiak, *JHEP* **03** (2016), 179 [[arXiv:1512.02472](#) [hep-ph]].
- [110] A. Bharucha, S. Heinemeyer and F. von der Pahlen, *Eur. Phys. J. C* **73** (2013) no.11, 2629 [[arXiv:1307.4237](#) [hep-ph]].
- [111] H. Baer, T. Krupovnickas, A. Mustafayev, E. K. Park, S. Profumo and X. Tata, *JHEP* **12** (2005), 011 [[arXiv:hep-ph/0511034](#) [hep-ph]].